

# Evidence that the AT transition disappears below six dimensions

Bharadwaj Vedula,<sup>1</sup> M. A. Moore,<sup>2</sup> and Auditya Sharma<sup>1</sup>

<sup>1</sup>*Department of Physics, Indian Institute of Science Education and Research, Bhopal, Madhya Pradesh 462066, India*

<sup>2</sup>*Department of Physics and Astronomy, University of Manchester, Manchester M13 9PL, United Kingdom*

(Dated: July 8, 2024)

One of the key predictions of Parisi's broken replica symmetry theory of spin glasses is the existence of a phase transition in an applied field to a state with broken replica symmetry. This transition takes place at the de Almeida-Thouless (AT) line in the  $h - T$  plane. We have studied this line in the power-law diluted Heisenberg spin glass in which the probability that two spins separated by a distance  $r$  interact with each other falls as  $1/r^{2\sigma}$ . In the presence of a random vector-field of variance  $h_r^2$  the phase transition is in the universality class of the Ising spin glass in a field. Tuning  $\sigma$  is equivalent to changing the dimension  $d$  of the short-range system, with the relation being  $d = 2/(2\sigma - 1)$  for  $\sigma < 2/3$ . We have found by numerical simulations that  $h_{\text{AT}}^2 \sim (2/3 - \sigma)$  implying that the AT line does not exist below 6 dimensions and that the Parisi scheme is not appropriate for spin glasses in three dimensions.

## I. INTRODUCTION

The relevance of the replica symmetry breaking (RSB) scheme of Parisi [1, 2] for physical spin glasses in three dimensions has occasioned doubts from its earliest days [3]. These doubts have mostly arisen from studies of the de Almeida-Thouless (AT) line [4]. This is the line in the field  $h$  and temperature  $T$  plane where the replica symmetric high-temperature phase changes to a phase with broken replica symmetry (see Fig. 1). The Parisi scheme has now been rigorously proved to solve the Sherrington-Kirkpatrick (SK) mean-field model [5], in which all spins interact with each other. In that model in the presence of a field  $h$ , the AT line  $h_{\text{AT}}(T)$  for temperatures  $T$  close to  $T_c$ , the zero-field transition temperature, takes the form

$$\left(\frac{h_{\text{AT}}(T)}{T_c}\right)^2 = A(d) \left(1 - \frac{T}{T_c}\right)^\zeta. \quad (1)$$

The exponent  $\zeta = 3$  in the SK model and remains at 3 for all  $d > 8$ . It takes the value  $d/2 - 1$  when  $8 > d > 6$  [6, 7]. For  $d < 6$ , should the AT line then still exist,  $\zeta = \gamma + \beta$ , where the exponent  $\gamma$  describes the divergence of the zero-field spin glass susceptibility  $\chi_{\text{SG}}$  as  $T \rightarrow T_c$ , and  $\beta$  describes how the Edwards-Anderson order parameter  $q_{\text{EA}}$  goes to zero in the same limit [7]. Both these zero-field exponents have an expansion in powers of  $\epsilon$  where  $d = 6 - \epsilon$  [8]. Back in 1980 Bray and Roberts [3] were unable to find a fixed point for the exponents at the AT line. One possibility which they suggested as an explanation was that for  $d < 6$  there simply was no AT line. However, the possibility that there was a non-perturbative fixed point could not be ruled out (but if such exists, it still remains to be discovered).

Another argument suggested long ago was that of Moore and Bray [10]. In  $d < 6$  the dependence on  $\gamma$  and  $\beta$  of the form of the AT line as  $\zeta = \gamma + \beta$  indicates that the applied field  $h$  has the scaling dimension of the ordering field of the spin glass. For  $d > 6$  that is not the case, as then  $\gamma + \beta = 2$  for all  $d > 6$ . Usually when the ordering field is present there is no phase transition. For

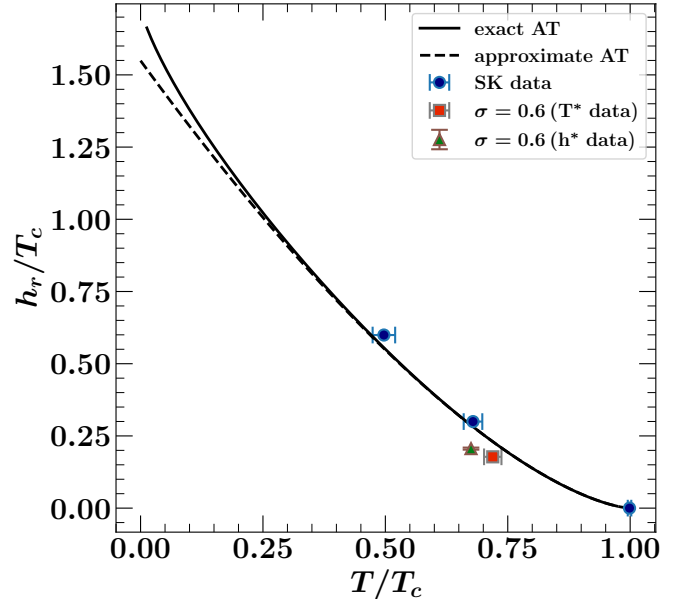


FIG. 1. The AT line. The solid line is the exact AT line for the SK model, calculated as in Ref. [9]. The dashed line is the approximation to it of Eq. (1) with  $\zeta = 3$ . Marked on the diagram by filled circles are the results of the simulations on the SK model in Ref. [9]. The red square point, derived from varying the temperature  $T$  at fixed  $h_r$ , and the upwards arrow point, derived from varying the field at fixed temperature, are the result of our simulations at  $\sigma = 0.6$ , which despite corresponding to 10 dimensions, have values of  $h_{\text{AT}}$  suppressed by fluctuations from those which would be estimated from the SK model when only adjusting the zero-field transition temperature  $T_c$ .

example, for a ferromagnet in its ordering field (which is a uniform field) there is no phase transition as the temperature is lowered. A phase transition only occurs for vanishing field. The suggestion of Moore and Bray was that because the applied field had the scaling dimensions of the ordering field in dimensions  $d < 6$  then there would also be no phase transition in a field and hence no AT

line when  $d < 6$  [10]. Even though it is commonplace that a phase transition is removed in the presence of the ordering field, alternatives are possible and some were discussed in Ref. [11], but no evidence for them was found.

Another argument that 6 might be the dimension above which RSB applies comes from RSB calculations of the interface free energy of the Ising spin glass in the presence of no external field. The calculations which are valid for  $d > 6$  are done for a system of length  $L$  in one direction and  $M$  in the other  $d - 1$  directions. The interface free energy  $\Delta F$  is the change in the free energy when the boundary conditions in the  $L$  direction are switched from periodic to anti-periodic [12, 13]. Its bond-average variance  $\Delta F^2$  is found to be of the form [13]

$$\Delta F^2 \sim N^{1/3} + L^2 f(L/M), \quad (2)$$

where  $N = LM^{d-1}$ . The leading term  $\sim N^{1/3}$  is of an unusual form for an interface free energy as it only depends on the volume or number of spins in the system, and is of this form because interfaces according to RSB are space filling as their fractal dimension  $d_s = d$ . The second term is of the conventional aspect ratio scaling form which involves the ratio of  $L/M$  usually associated with interfaces whose fractal dimensions  $d_s$  are less than  $d$  and which are not space filling [14, 15]. Using a simple (and approximate) renormalization group procedure it has been found that  $d_s \rightarrow d$  as  $d \rightarrow 6$  from below [16]. The term  $L^2 f(L/M)$  becomes  $L^{2\theta} f(L/M)$  for  $d < 6$ , and then the first term will not be present.  $\theta$  is the interface free energy exponent [14]. According to the numerical study of Boettcher [17]  $\theta = 1.1(1)$  in six dimensions, which suggests it might be exactly 1 when  $d = 6$ . But the crucial point is that for  $d > 6$  the first term dominates, but the second term becomes just as large as the first term right in  $d = 6$  for  $L \sim M$ . This suggests that  $d = 6$  is at least an important dimension for RSB in spin glasses and possibly its lower critical dimension, the dimension below which full replica symmetry breaking of the Parisi type is no longer to be found.

Interface free energies are determined by the nature of the zero-temperature fixed point of the system and its associated exponents such as  $\theta$ . These exponents should be distinguished from those associated with the critical fixed point. The study of Bray and Roberts [3] was an expansion about the upper critical dimension of the AT line, which was taken to be 6. The argument of this paper that there is no RSB for  $d \leq 6$ , which if valid implies that the upper and lower critical dimensions for RSB behavior are both the same and equal to 6 – a most unusual situation!

If the lower critical dimension for the existence of the AT line is six, then one would expect that the AT line will become closer to the temperature axis as  $d \rightarrow 6$ . To see whether this is the case requires determination of the coefficient  $A(d)$ , but this is very challenging. In the SK limit for unit length  $m$ -component vector spins,  $A(d) = 4m/(m+2)$ : For the Heisenberg model studied in

this paper  $m = 3$ . By using an expansion in  $1/m$ , Moore argued that as  $d \rightarrow 6$  from above  $A(d) \sim (d-6)$  [18]. The numerical studies reported in this paper are consistent with this possibility. They indeed imply therefore that the AT line is approaching the temperature axis as  $d \rightarrow 6$ , and hence that there will not be an AT transition below six dimensions.

The question of whether there is or is not an AT line in physical dimensions such as  $d = 3$  has naturally been studied by both experiment and by simulations. On the experimental side a negative answer was suggested by the work in Ref. [19], while a positive answer was provided in Ref. [20]. No consensus is found in simulations either: for a recent review see [21].

Because it is hard to do simulations above 6 dimensions (although recently an attempt was made to study the AT line in 6 dimensions [22]), we have done simulations on the one-dimensional proxy model where systems of large linear extent  $L$  can be studied. In Ref. [22] where a six-dimensional version was directly simulated,  $L$  was less than 8, but we can study values of  $L$  up to 65536.

We organised the paper into the following sections. In Sec. II we describe the model we used in detail. The quantities we studied and their finite size scaling forms near the AT transition point are given in Sec. III. In Sec. IV we show the results obtained by performing finite size scaling analyses on the data for five values of  $\sigma$  in the mean-field regime: 0.600, 0.630, 0.640, 0.650, and 0.655. In Sec. V, we show our analysis of  $A(\sigma)$  versus  $\sigma$  which provided us strong evidence that the AT line disappears below  $\sigma_c = 2/3$ . In an earlier investigation on the XY model [23] we had studied it for  $\sigma$  values 0.60, 0.70, 0.75 and 0.85, and had observed that because the leading correction to scaling exponent  $\omega$  approaches 0 as  $\sigma \rightarrow \sigma_c = 2/3$  it would be very challenging to determine whether the AT line goes away precisely at  $\sigma = 2/3$ . This means that as  $\sigma \rightarrow 2/3$  one needs to go to ever larger values of the system size  $N$  to maintain the same level of accuracy. Finally in Sec. VI we summarize our conclusions.

## II. MODEL HAMILTONIAN

The Hamiltonian of our system is

$$\mathcal{H} = - \sum_{\langle i,j \rangle} J_{ij} \mathbf{S}_i \cdot \mathbf{S}_j - \sum_i \mathbf{h}_i \cdot \mathbf{S}_i, \quad (3)$$

where  $\mathbf{S}_i$ , a unit vector of  $m = 3$  components, is a spin sitting on the  $i^{\text{th}}$  lattice site ( $i = 1, 2, \dots, N$ ). The  $N$  ( $\equiv L$ ) lattice sites are arranged around a ring of circumference  $N$ . So the distance between the spins at sites  $i$  and  $j$  [26]

$$r_{ij} = \frac{N}{\pi} \sin \left( \frac{\pi}{N} |i - j| \right), \quad (4)$$

is the length of the chord connecting them. The probability of having a non-zero interaction between a pair of

spins  $(i, j)$  falls with the distance  $r_{ij}$  between the spins as a power law:

$$p_{ij} = \frac{r_{ij}^{-2\sigma}}{\sum_{j \neq i} r_{ij}^{-2\sigma}}. \quad (5)$$

The interactions  $J_{ij}$  between a pair of spins  $(i, j)$  are independent Gaussian random variables with mean zero and standard deviation unity, i.e:

$$[J_{ij}]_{\text{av}} = 0 \quad \text{and} \quad [J_{ij}^2]_{\text{av}} = J^2 = 1. \quad (6)$$

The Cartesian components  $h_i^\mu$  of the on-site external field are independent random variables drawn from a Gaussian distribution of zero mean with each component having variance  $h_r^2$ . The detailed prescription to generate such a lattice with long-range diluted interactions is given in references [23, 24, 27].

This model has already been extensively studied. Even though it involves spins of  $m$  ( $= 3$ ) components, its AT transition is in the universality class of the Ising ( $m = 1$ ) model [9]. Despite the additional degrees of freedom of the spins compared to those of the Ising model, the Heisenberg model is easier to simulate than the Ising model as the vector spins provide a means to go around barriers rather than over them as in the Ising case, allowing larger systems to be simulated [28]. In the interval  $1/2 < \sigma < 2/3$ , it corresponds to an Edwards-Anderson short-range model in  $d_{\text{eff}}$  dimensions [26], where

$$d_{\text{eff}} = \frac{2}{2\sigma - 1}. \quad (7)$$

Thus if  $\sigma = 0.6$  (see Fig. 1),  $d_{\text{eff}} = 10$ . We ourselves have extensively studied the XY ( $m = 2$ ) version of it [23], when we concentrated mainly on cases where  $\sigma > 2/3$ . Since writing that paper we have discovered that the Heisenberg case ( $m = 3$ ) runs faster, enabling us to study larger systems. In this paper we have focussed on cases  $\sigma < 2/3$  corresponding to  $d > 6$  in an attempt to determine whether the AT line vanishes as  $d \rightarrow 6$ . At the time of writing of our paper on the XY spin glass model, we thought determining whether the AT line vanished as  $\sigma \rightarrow 2/3$  would be very challenging as the corrections to scaling become larger and larger in this limit, requiring the study of increasingly larger values of  $N$  to achieve the equivalent level of accuracy. Our work in this paper is indeed affected by this difficulty which prevents us getting really close to  $\sigma = 2/3$  but it does suggest that the AT line might vanish at  $d = 6$  (i.e.  $\sigma = 2/3$ ) if the limit  $N \rightarrow \infty$  could be studied.

### III. CORRELATION LENGTHS AND SUSCEPTIBILITIES

As in the XY case we shall focus on the wave-vector-dependent spin glass susceptibility [24]

$$\chi_{\text{SG}}(k) = \frac{1}{N} \sum_{i,j} \frac{1}{m} \sum_{\mu,\nu} \left[ (\chi_{ij}^{\mu\nu})^2 \right]_{\text{av}} e^{ik(i-j)}, \quad (8)$$

where

$$\chi_{ij}^{\mu\nu} = \langle S_i^\mu S_j^\nu \rangle - \langle S_i^\mu \rangle \langle S_j^\nu \rangle. \quad (9)$$

From it the spin glass correlation length is then determined using the relation

$$\xi_{\text{SG}} = \frac{1}{2 \sin(k_{\text{min}}/2)} \left( \frac{\chi_{\text{SG}}(0)}{\chi_{\text{SG}}(k_{\text{min}})} - 1 \right)^{1/(2\sigma-1)}, \quad (10)$$

and  $k_{\text{min}} = 2\pi/N$ . The spin glass susceptibility itself is  $\chi_{\text{SG}} = \chi_{\text{SG}}(0)$ . The simulations and equilibration checks were performed according to the procedures outlined in Ref. [9, 28], with the details provided in Appendix A.

At the AT transition, both  $\chi_{\text{SG}}$  and  $\xi_{\text{SG}}$  diverge to infinity. For  $\sigma < 2/3$  the finite size scaling form when approaching the AT line along a vertical trajectory (i.e. by varying  $h_r$ ) for a finite value of  $N$  [23] is:

$$\frac{\chi_{\text{SG}}}{N^{1/3}} = \mathcal{C} \left[ N^{1/3} (h_r - h_{\text{AT}}(T)) \right] + N^{-\omega} \mathcal{G} \left[ N^{1/3} (h_r - h_{\text{AT}}(T)) \right]. \quad (11)$$

The second term is a correction to scaling term. The exponent  $\omega$  is given by [9, 29]

$$\omega = 1/3 - (2\sigma - 1). \quad (12)$$

Notice that as  $\sigma \rightarrow 2/3$ ,  $\omega \rightarrow 0$ . This is why it is so challenging to show that the AT line disappears as  $d \rightarrow 6$ . The finite size scaling form for  $\xi_{\text{SG}}$  is [23]

$$\frac{\xi_{\text{SG}}}{N^{d_{\text{eff}}/6}} = \mathcal{X} \left[ N^{1/3} (h_r - h_{\text{AT}}(T)) \right] + N^{-\omega} \mathcal{H} \left[ N^{1/3} (h_r - h_{\text{AT}}(T)) \right]. \quad (13)$$

In the absence of the correction to scaling term the plots of  $\chi_{\text{SG}}/N^{1/3}$  or  $\xi_{\text{SG}}/N^{d_{\text{eff}}/6}$  for different system sizes would intersect at  $h_r = h_{\text{AT}}(T)$ . The intersection formula for the successive crossing points  $h^*(N, 2N)$  should be linear in  $1/N^\lambda$  when  $N \rightarrow \infty$  and be of the form

$$h^*(N, 2N) = h_{\text{AT}}(T) + \frac{A}{N^\lambda}, \quad (14)$$

where

$$\lambda = 1/3 + \omega. \quad (15)$$

We have not only studied  $\chi_{\text{SG}}$  and  $\xi_{\text{SG}}$  as a function of  $h_r$  at fixed  $T$  but we have also studied them as a function of  $T$  for fixed  $h_r = 0$ . We did the latter to determine the zero-field transition temperature  $T_c$ . The relevant finite size scaling forms for this situation are

$$\frac{\chi_{\text{SG}}}{N^{1/3}} = \tilde{\mathcal{C}} \left[ N^{1/3} (T - T_c) \right] + N^{-\omega} \tilde{\mathcal{G}} \left[ N^{1/3} (T - T_c) \right], \quad (16)$$

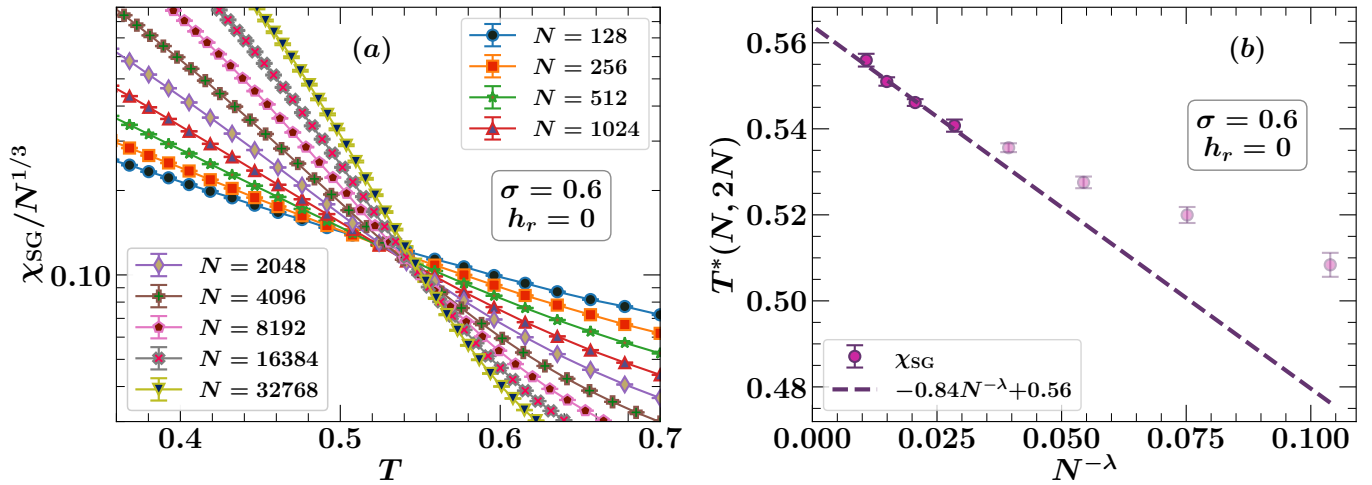


FIG. 2. Finite size scaling analyses of data for  $\sigma = 0.600$  obtained by varying the temperature in the absence of a magnetic field. (a) shows the plot of  $\chi_{\text{SG}}/N^{1/3}$  as a function of the temperature  $T$  for different system sizes. The plot shows that the curves for different system sizes intersect. The data for the intersection temperatures  $T^*(N, 2N)$  between pairs of adjacent system sizes are plotted as a function of  $N^{-\lambda}$  in (b). The value of the exponent  $\lambda$  is fixed to be 0.467 which is known exactly in the mean-field regime [24, 25]. We fitted the  $T^*(N, 2N)$  data with Eq. (18) using linear fitting and the resulting value of the transition temperature is  $T_c = 0.5639 \pm 0.0020$  (see Table I for details). The blurred points in (b) are excluded in from the linear fitting.

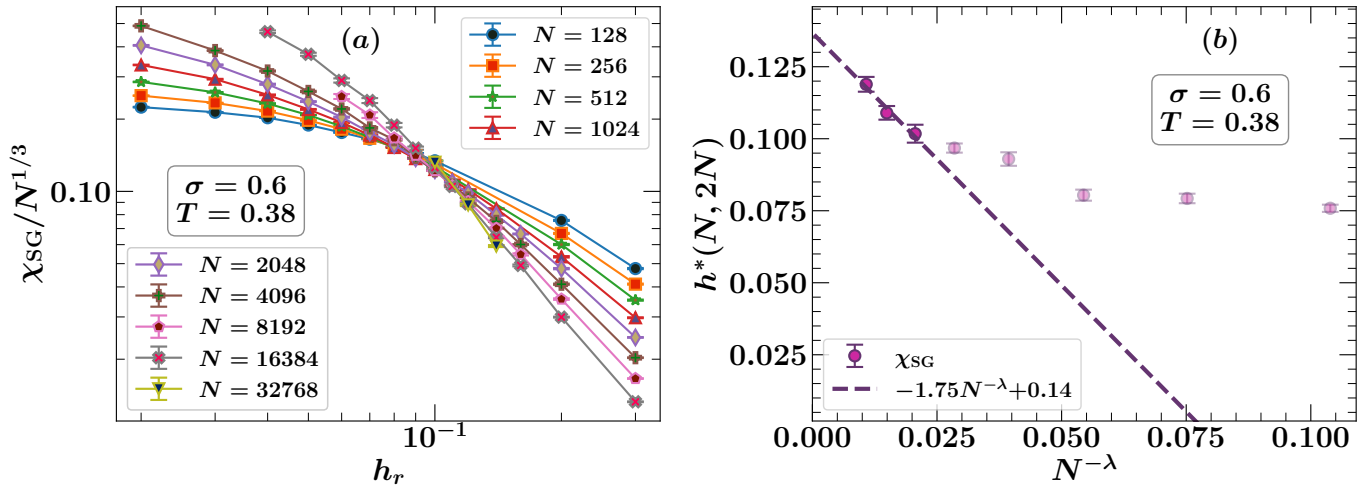


FIG. 3. (a) Finite size scaling analyses of  $\chi_{\text{SG}}$  data for  $\sigma = 0.600$  obtained by fixing the temperature to  $T = 0.380 (= 0.674 T_c)$  and varying the field. The plot shows that the curves for different system sizes intersect. (b) shows the data for the intersection fields  $h^*(N, 2N)$  between pairs of adjacent system sizes, plotted as a function of  $N^{-\lambda}$ . Using  $\lambda = 0.467$  we fitted the  $h^*(N, 2N)$  data linearly with Eq. (14) and the value of the transition field so obtained is  $h_{\text{AT}}(T = 0.380) = 0.1367 \pm 0.0063$  (see Table II for details). The blurred points in (b) are excluded from the linear fitting.

and

$$\frac{\xi_{\text{SG}}}{N^{d_{\text{eff}}/6}} = \tilde{\chi} \left[ N^{1/3}(T - T_c) \right] + N^{-\omega} \tilde{\mathcal{H}} \left[ N^{1/3}(T - T_c) \right]. \quad (17)$$

The tilde sign is to indicate that the finite size scaling functions such as  $\mathcal{C}$  in a field and  $\tilde{\mathcal{C}}$  in the absence of a field may differ.

The intersection points as in, say, Fig. 4 (b) would be

expected to be of the form

$$T^*(N, 2N) = T_c + \frac{\tilde{A}}{N^\lambda}. \quad (18)$$

Note that the values of the exponents  $\omega$  and  $\lambda$  are the same for the zero field transition and for the AT line (assuming that they are both governed by a Gaussian fixed point).

In section IV we give the results of our studies of  $\chi_{\text{SG}}$  for values of  $\sigma$  at 0.600, 0.630, 0.640, 0.650 and 0.655. We

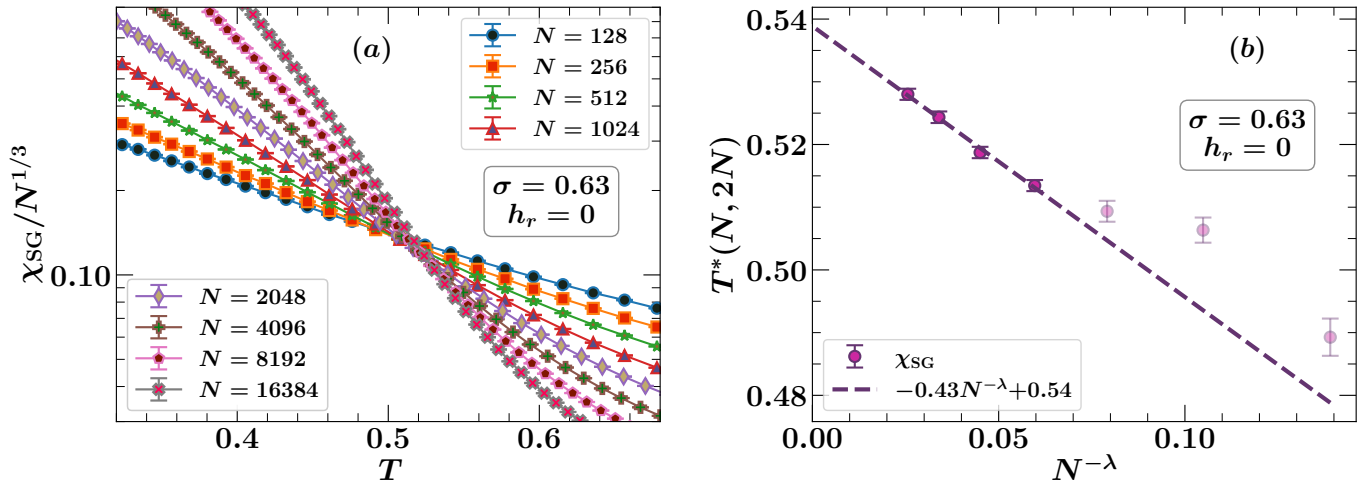


FIG. 4. Finite size scaling analyses of data for  $\sigma = 0.630$  obtained by varying the temperature in the absence of a magnetic field. (a) shows the plot of  $\chi_{\text{SG}}/N^{1/3}$  as a function of the temperature  $T$  for different system sizes. The data for the intersection temperatures  $T^*(N, 2N)$  between pairs of adjacent system sizes are plotted as a function of  $N^{-\lambda}$  in (b). The value of the exponent  $\lambda$  is fixed to be 0.407. The line fit gives  $T_c = 0.5389 \pm 0.0015$  (see Table I for details). The blurred points in (b) are excluded from the linear fitting.

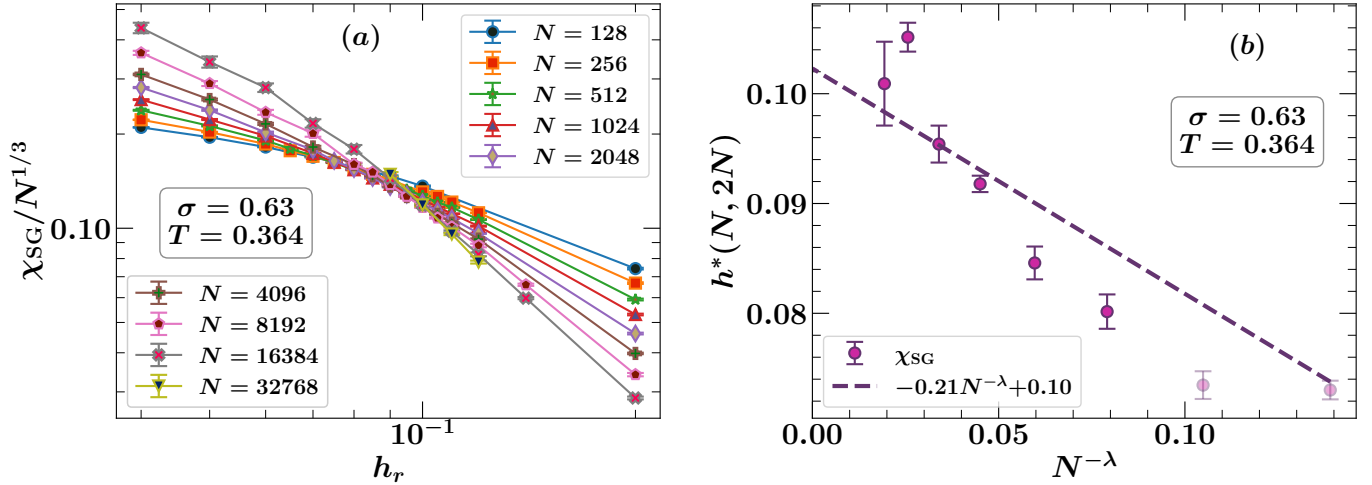


FIG. 5. (a) Finite size scaling analyses of  $\chi_{\text{SG}}$  data for  $\sigma = 0.630$  obtained by fixing the temperature to  $T = 0.364 (= 0.675 T_c)$  and varying the field. (b) shows the data for the intersection fields  $h^*(N, 2N)$  plotted as a function of  $N^{-\lambda}$ . Using  $\lambda = 0.407$  we fitted the  $h^*(N, 2N)$  data linearly with Eq. (14) and the value of the transition field so obtained is  $h_{\text{AT}}(T = 0.364) = 0.1172 \pm 0.0022$  (see Table II for details). The blurred points in (b) are excluded from the linear fitting.

also describe how the zero-field transition temperature  $T_c$  was determined for each of these values of  $\sigma$ . The results obtained from  $\xi_{\text{SG}}$  corresponding to the same values of  $\sigma$  are given in Appendix C.

Leuzzi et al. [30] pointed out that determination of  $\xi_{\text{SG}}$  was especially badly affected by finite size effects. They found that if it were calculated not from the two  $k$  values which we used, 0 and  $k_{\text{min}}$ , but instead two non-zero values,  $k_1$  and  $k_2$ , a different value for  $\xi_{\text{SG}}$  was obtained. In a recent paper Aguilar-Janita et al. [22] pointed out that in zero field the two methods gave the same result, and only differed in a field. They attributed the difference to the fact that when studying the AT line one requires the

field to be large enough so that the Parisi overlap function  $P(q)$  vanishes for  $q < 0$ . This requires  $\sqrt{q}h_r\sqrt{N} > k_B T$ . When this criterion is not satisfied there are additional crossovers and length scales beyond those discussed in this section. As we find that the field at the AT line is approaching zero as  $\sigma \rightarrow 2/3$  the criterion requires the study of even larger system sizes as  $\sigma \rightarrow 2/3$ , which makes our results from  $\xi_{\text{SG}}$  especially unreliable and it is for this reason we have relegated them to Appendix C. Finite size effects affect some quantities more than others and hopefully our estimates of  $h_{\text{AT}}$  from  $\chi_{\text{SG}}$  are less affected. This might be because the values of  $\chi_{\text{SG}}/N^{1/3}$  in zero field and on the AT line are rather similar, whereas

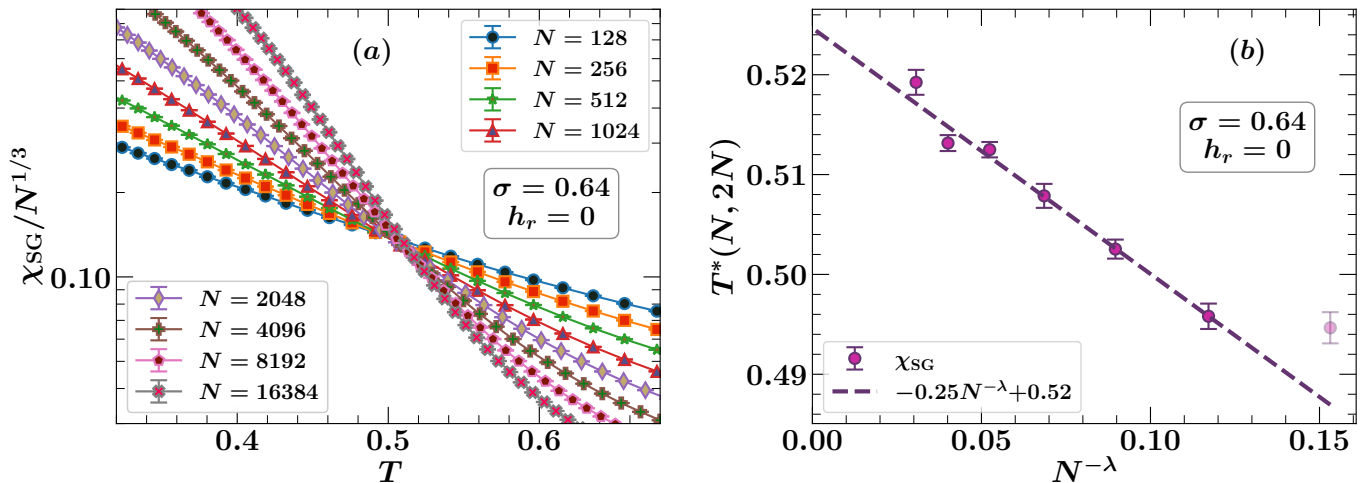


FIG. 6. (a) Finite size scaling analyses of  $\chi_{\text{SG}}$  data for  $\sigma = 0.640$  obtained by varying the temperature in the absence of a magnetic field. (b) shows the data for the intersection temperatures  $T^*(N, 2N)$  plotted as a function of  $N^{-\lambda}$  with  $\lambda = 0.387$ . The line fit gives  $T_c = 0.5247 \pm 0.0010$  (see Table I for details). The blurred point in (b) is excluded from the linear fitting.

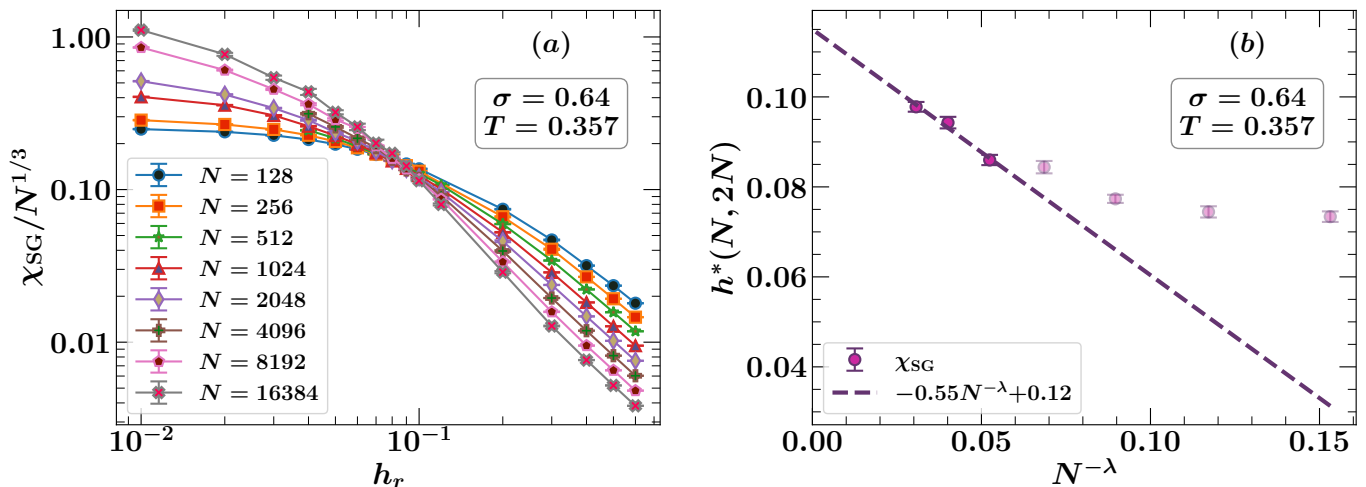


FIG. 7. (a) Finite size scaling analyses of  $\chi_{\text{SG}}$  data for  $\sigma = 0.640$  obtained by fixing the temperature to  $T = 0.357$  ( $= 0.680 T_c$ ) and varying the field. (b) shows the data for the intersection fields  $h^*(N, 2N)$  between pairs of adjacent system sizes, fitted against  $N^{-\lambda}$ , using  $\lambda = 0.387$ . The value of the transition field so obtained is  $h_{\text{AT}}(T = 0.357) = 0.1150 \pm 0.0030$  (see Table II for details). The blurred points in (b) are excluded from the linear fitting.

the values of  $\xi_{\text{SG}}/N^{d_{\text{eff}}/6}$  on the AT line are larger than their values in zero field by a factor of order 10.

#### IV. FINITE SIZE SCALING ANALYSES

Here we give further details of the results of our simulations for  $\sigma$  values 0.600, 0.630, 0.640, 0.650 and 0.655. Figs. 2, 4, 6, 8, and 10 show the finite size scaling analyses of data for these different values of  $\sigma$  obtained by varying the temperature in the absence of a magnetic field. In all these figures, Figs. (a) show the plot of  $\chi_{\text{SG}}/N^{1/3}$  as a function of the temperature  $T$  for different system sizes. In all these sets of plots we can clearly notice that the curves for different system sizes intersect around the tran-

sition temperature, which is in accordance with Eq. (16). For each pair of adjacent system sizes, we find the intersection temperature  $T^*(N, 2N)$  from  $\chi_{\text{SG}}$  data which is the  $x$ -coordinate corresponding to the point of intersection between these curves. The data for the intersection temperatures obtained from all the pairs of adjacent system sizes are plotted as a function of  $N^{-\lambda}$  in Figs. (b). The value of the exponent  $\lambda$  is known in the mean-field regime and is given by Eq. (15) [24, 25]. Using this value of  $\lambda$  we fit the  $T^*(N, 2N)$  data linearly with Eq. (18) for the  $N_{\text{pairs}}$  largest pairs of system sizes. In the thermodynamic limit  $N^{-\lambda} \rightarrow 0$  as  $N \rightarrow \infty$ . Hence, the  $y$ -intercept corresponding to the straight line fit gives us the value of the zero-field transition temperature  $T_c$ . The values of  $T_c$  obtained for different values of  $\sigma$  are shown in Table I,

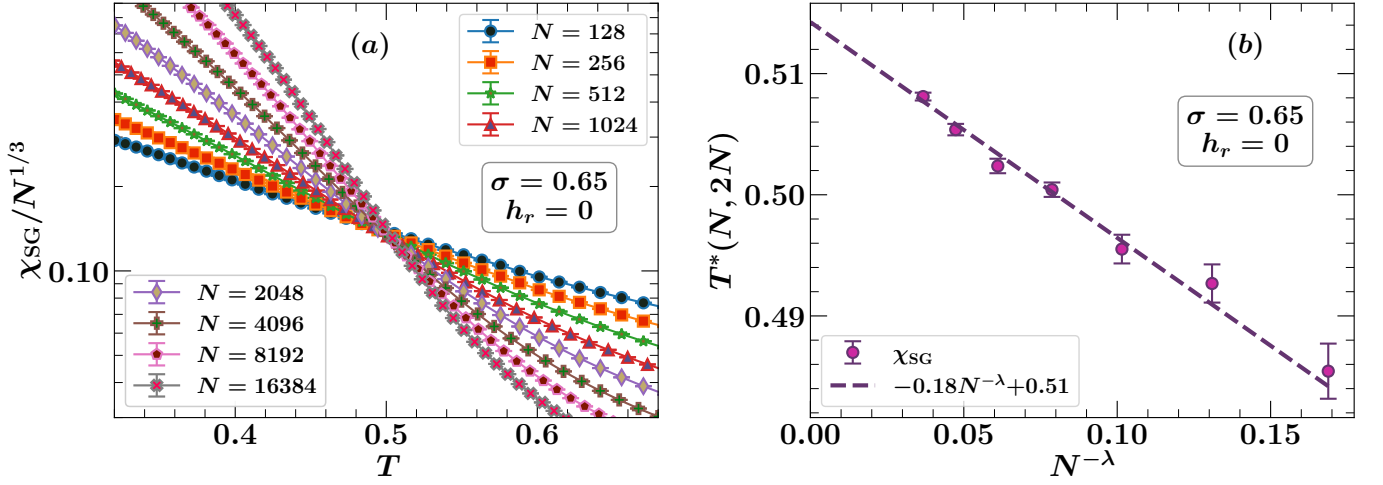


FIG. 8. (a) Finite size scaling analyses of  $\chi_{\text{SG}}$  data for  $\sigma = 0.650$  obtained by varying the temperature in the absence of a magnetic field. The data for the intersection temperatures  $T^*(N, 2N)$  are plotted as a function of  $N^{-\lambda}$  (using  $\lambda = 0.367$ ) in (b). The value of the zero-field transition temperature obtained from linear fitting is  $T_c = 0.5143 \pm 0.0005$  (see Table I for details).

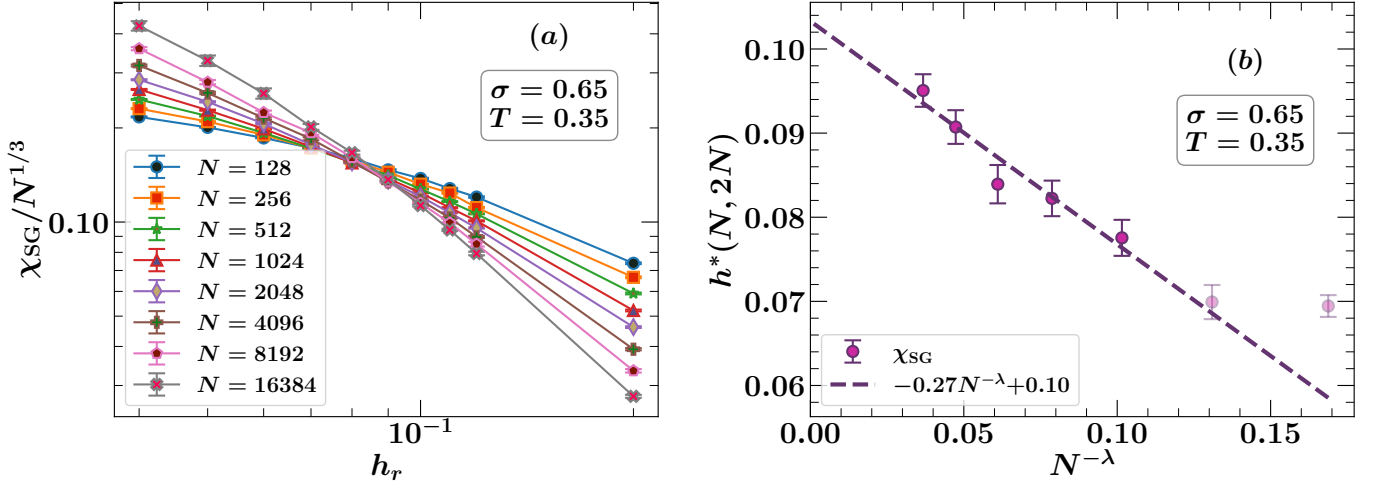


FIG. 9. (a) Finite size scaling analyses of  $\chi_{\text{SG}}$  data for  $\sigma = 0.650$  obtained by fixing the temperature to  $T = 0.350$  ( $= 0.681 T_c$ ) and varying the field. (b) shows the data for the intersection fields  $h^*(N, 2N)$  between pairs of adjacent system sizes, plotted as a function of  $N^{-\lambda}$ . Using  $\lambda = 0.367$  we fitted the  $h^*(N, 2N)$  data linearly with Eq. (14) and the value of the transition field so obtained is  $h_{\text{AT}}(T = 0.350) = 0.1033 \pm 0.0027$  (see Table II for details). The blurred points in (b) are excluded from the linear fitting.

and the parameters of the simulations are shown in Table BI.

The AT line can be approached not only by reducing the temperature  $T$  but also by reducing the field at fixed  $T$ . This was the procedure used in Ref. [23]. These are the vertical trajectories in Fig. 1 along which we can cross the AT line. Throughout this paper, we chose the value of temperature  $T$  such that  $T/T_c \approx 0.67$ . We show our finite size scaling analyses plots corresponding to this procedure in Figs. 3, 5, 7, 9, and 11. Similar to the zero-magnetic field case, we present our  $\chi_{\text{SG}}$  data in Fig. (a) as a function of magnetic field  $h_r$ . According to Eq. (11), the data for  $\chi_{\text{SG}}/N^{1/3}$  when plotted for dif-

ferent system sizes should intersect at the AT transition field  $h_{\text{AT}}(T)$ . Figs. (b) show the data for the intersection fields  $h^*(N, 2N)$  obtained by considering the curves for adjacent system sizes. We fit the  $h^*(N, 2N)$  data with Eq. (14) through a straight line for the  $N_{\text{pairs}}$  largest pairs of system sizes using the same value of  $\lambda$  as in the previous scenario, which is given by Eq. (15). The point at which this straight line cuts the  $y$ -axis gives us the value of the transition field  $h_{\text{AT}}$  corresponding to the temperature  $T$ . The values of  $h_{\text{AT}}$  obtained for different  $\sigma$  are shown in Table II, and the parameters of the simulation are shown in Table BII.

We have also performed finite size scaling analyses on

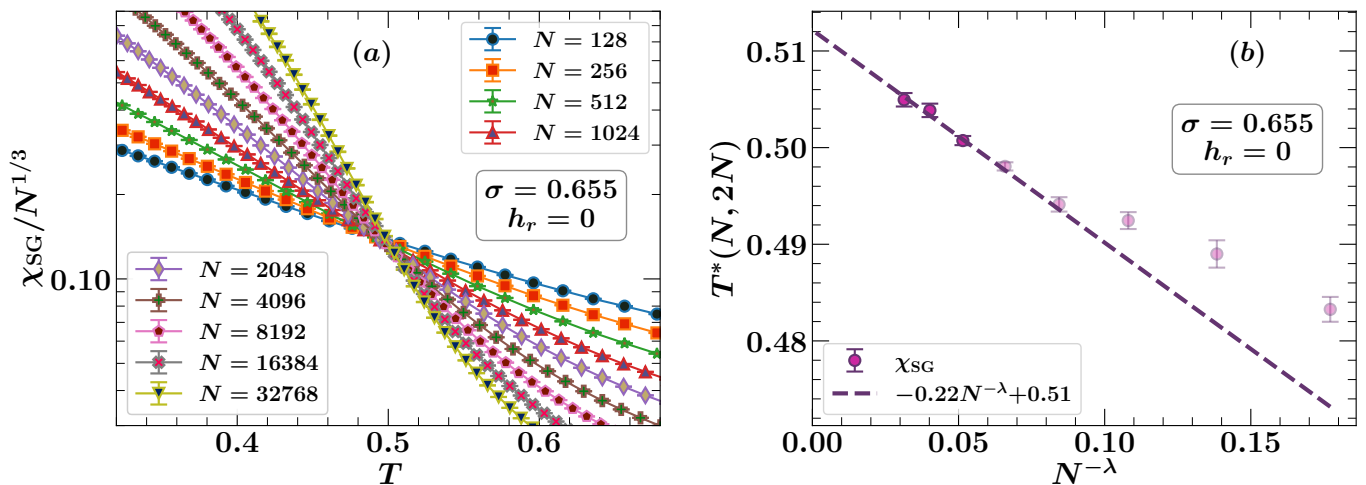


FIG. 10. (a) Finite size scaling analyses of  $\chi_{\text{SG}}$  data for  $\sigma = 0.655$  obtained by varying the temperature in the absence of a magnetic field. (b) shows the data for the intersection temperatures  $T^*(N, 2N)$  fitted against  $N^{-\lambda}$ . The value of the exponent  $\lambda$  is fixed to be 0.357. The line fit gives  $T_c = 0.5122 \pm 0.0018$  (see Table I for details). The blurred points in (b) are excluded from the linear fitting.

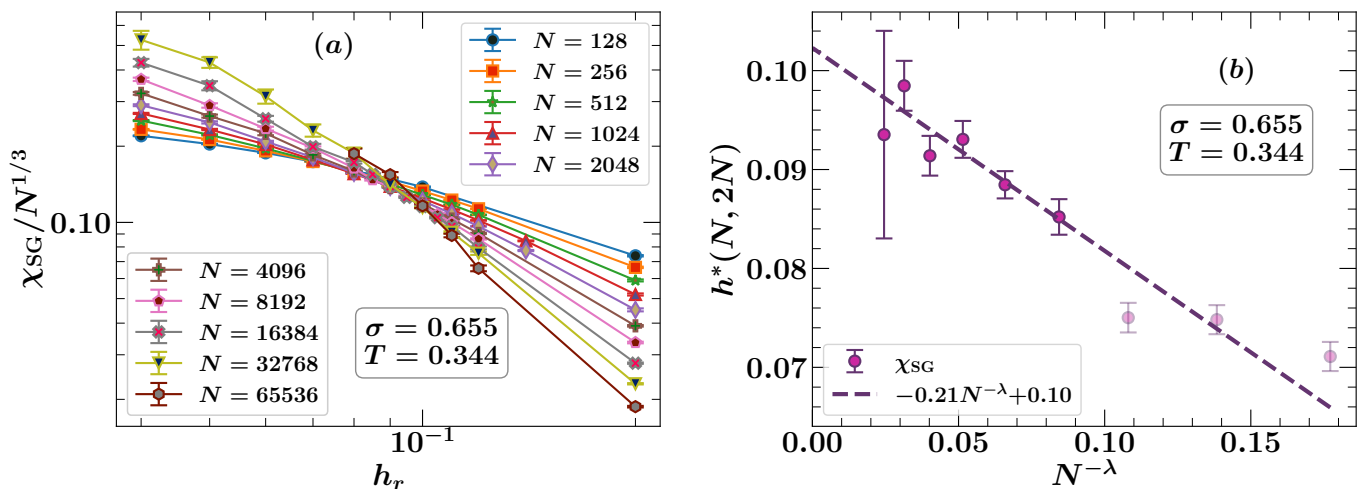


FIG. 11. (a) Finite size scaling analyses of  $\chi_{\text{SG}}$  data for  $\sigma = 0.655$  obtained by fixing the temperature to  $T = 0.344 (= 0.672 T_c)$  and varying the field. In (b) the data for the intersection fields  $h^*(N, 2N)$  is plotted as a function of  $N^{-\lambda}$  with  $\lambda = 0.357$ . We fitted the  $h^*(N, 2N)$  data with a straight line and the value of the transition field obtained as a result of the extrapolation of the straight line is  $h_{\text{AT}}(T = 0.344) = 0.1023 \pm 0.0029$  (see Table II for details). The blurred points in (b) are excluded from the linear fitting.

$\xi_{\text{SG}}$  data for all the 5 values of  $\sigma$  both in the zero field case and by varying the field at a fixed temperature. Similar to  $\chi_{\text{SG}}$  we plotted  $\xi_{\text{SG}}/N^{d_{\text{eff}}/6}$  for different system sizes as a function of temperature  $T$  for  $h_r = 0$ , with  $d_{\text{eff}} = 2/(2\sigma - 1)$ , and obtained the values of intersection temperatures  $T^*(N, 2N)$ . As for the vertical trajectory, we fixed  $T \approx 0.67 T_c$  and, plotted  $\xi_{\text{SG}}/N^{d_{\text{eff}}/6}$  as a function of field  $h_r$ , and computed the values of intersection fields  $h^*(N, 2N)$ . We then analysed the intersection temperatures or fields data as a function of  $N^{-\lambda}$  with  $\lambda$  being the same for both  $T^*$  and  $h^*$  data sets obtained from both  $\chi_{\text{SG}}$  and  $\xi_{\text{SG}}$ . Upon doing linear fitting we obtained the values of  $T_c$  and  $h_{\text{AT}}(T)$  from the  $T^*$  and  $h^*$  data sets

respectively. We presented our  $\xi_{\text{SG}}$  data in Appendix C. In the following sections we present the results of finite size scaling analyses on  $\chi_{\text{SG}}$  data for different values of  $\sigma$ .

#### A. $\sigma = 0.600$

At  $\sigma = 0.600$ , for which  $d_{\text{eff}} = 10$  the results should be quite close to those of the SK model (but see Fig. 1): it is in the same mean-field regime and the exponent  $\zeta = 3$ . The zero-field transitions for this case has been studied by one of the authors of this paper in Ref. [24] for Heisen-



TABLE I. Results of the simulations done by varying the temperature  $T$  in the absence of magnetic field  $h_r$ . The  $\chi_{\text{SG}}/N^{1/3}$  when plotted as a function of temperature  $T$ , the data for different system sizes  $N$  intersect around the transition temperature  $T_c(\chi_{\text{SG}})$ . The intersection temperatures  $T^*(N, 2N)$  between the curves for two adjacent system sizes are then plotted as a function of  $N^{-\lambda}$ , with  $\lambda = 5/3 - 2\sigma$  in the mean field regime [24, 25]. We then fit this data for the  $N_{\text{pairs}}$  largest pairs of system sizes with Eq. (18) to find the transition temperature  $T_c(\chi_{\text{SG}})$ . For linear fitting, we attempt to fit the intersection data with a straight line for various values of  $N_{\text{pairs}}$ , and we choose the best fit where  $\chi^2/N_{\text{dof}}$  is closest to one.

$\sigma$	$h_r$	$\lambda$	$N_{\text{pairs}}(\chi_{\text{SG}})$	$T_c(\chi_{\text{SG}})$	$\chi^2/N_{\text{dof}}$
0.600	0	0.467	4	$0.5639 \pm 0.0020$	0.6832
0.630	0	0.407	4	$0.5389 \pm 0.0015$	0.4176
0.640	0	0.387	6	$0.5247 \pm 0.0010$	2.0093
0.650	0	0.367	7	$0.5143 \pm 0.0005$	1.4155
0.655	0	0.357	3	$0.5122 \pm 0.0018$	0.8398

TABLE II. Results of the simulations done by varying the magnetic field  $h_r$  at a fixed temperature  $T$ .  $T_c$  is the zero-field spin glass transition temperature obtained from the last column of the Table I. Similar to the fixed  $h_r$  case described in Table I, we plot the finite-size-scaled  $\chi_{\text{SG}}$  data as a function of the field  $h_r$  and find the intersection fields  $h^*(N, 2N)$ . We then fit this data for the  $N_{\text{pairs}}$  largest pairs of system sizes with Eq. (14) to find the AT transition field  $h_{\text{AT}}$  corresponding to the temperature  $T$ . For linear fitting, we attempt to fit the intersection data with a straight line for various values of  $N_{\text{pairs}}$ , and we choose the best fit where  $\chi^2/N_{\text{dof}}$  is closest to one.

$\sigma$	$T$	$T_c$	$T/T_c$	$\lambda$	$N_{\text{pairs}}(\chi_{\text{SG}})$	$h_{\text{AT}}(\chi_{\text{SG}})$	$\chi^2/N_{\text{dof}}$
0.600	0.380	0.564	0.674	0.467	3	$0.1367 \pm 0.0063$	0.7693
0.630	0.364	0.539	0.675	0.407	5	$0.1172 \pm 0.0022$	2.7216
0.640	0.357	0.525	0.680	0.387	3	$0.1150 \pm 0.0030$	1.1371
0.650	0.350	0.514	0.681	0.367	5	$0.1033 \pm 0.0027$	0.9507
0.655	0.344	0.512	0.672	0.357	6	$0.1023 \pm 0.0029$	0.8777

berg spins. As a sanity check, we attempted to replicate this analysis, and the results, displayed in Fig. 2, are in complete agreement with those presented in Ref. [24]. The value of the zero-field spin glass transition temperature found from these simulations is  $T_c = 0.564$ . The phase transitions in the presence of an external magnetic field has also been studied in Ref. [31] for  $h_r = 0.1$ . It has been reported that the system undergoes a phase transition at  $T_{\text{AT}}(h_r = 0.1) = 0.406$ .

For  $\sigma = 0.600$  we fixed the temperature at  $T = 0.380 (= 0.674 T_c)$ . We have constructed the crossing plots for  $\chi_{\text{SG}}$  as a function of  $h_r$  in Fig. 3(a). Analysis of the crossing points  $h^*(N, 2N)$  in Fig. 3(b) shows that the behavior is again consistent with the existence of an AT line at least at  $\sigma = 0.600$ . The value of the exponent  $\lambda$  is known in the mean-field regime and is given by  $\lambda = 5/3 - 2\sigma = 0.467$ . The  $h^*(N, 2N)$  data for the largest 3 pairs of system sizes are fitted against  $N^{-\lambda}$  to give  $h_{\text{AT}}(T = 0.380) = 0.1367 \pm 0.0063$  (see Table II).

### B. $\sigma = 0.630$

For  $\sigma = 0.630$   $d_{\text{eff}} \approx 7.692$ . Our results for  $h_r = 0$  are given in Fig. 4. According to Eq. (16), the data for  $\chi_{\text{SG}}/N^{1/3}$  when plotted for different system sizes should

intersect at the transition temperature  $T_c$ . Fig. 4(a) shows the data for different system sizes. We find the temperature  $T^*(N, 2N)$  at which the curves corresponding to the system sizes  $N$  and  $2N$  intersect. We then fit this data with Eq. (18) to find the transition temperature. The exponent  $\lambda \equiv 5/3 - 2\sigma$  is known to equal 0.407 in this case. The result is displayed in Fig. 4(b), where the  $T^*(N, 2N)$  data obtained from intersections of  $\chi_{\text{SG}}$  are fitted against  $N^{-\lambda}$  with a straight line for the largest 4 pairs of system sizes to give  $T_c = 0.5389 \pm 0.0015$  (see Table I).

We have also studied  $\chi_{\text{SG}}$  at fixed  $T$ , but varying  $h_r$  and the finite size scaling plots for these are given in Fig. 5(a). There appears to be good intersections in the curves, supporting therefore the possible existence of an AT transition at the temperature studied  $T = 0.364$ . A plot of  $h^*(N, 2N)$  versus  $1/N^\lambda$  is in Fig. 5(b), using the same value of  $\lambda = 0.407$ . Considering the data for the 5 largest pairs of system sizes, we did a linear fitting over the  $h^*(N, 2N)$  data obtained from  $\chi_{\text{SG}}$  intersections, which gives  $h_{\text{AT}}(T = 0.364) = 0.1172 \pm 0.0022$  (see Table II).

### C. $\sigma = 0.640$

For  $\sigma = 0.640$ ,  $d_{\text{eff}} \approx 7.143$ . Our results for  $h_r = 0$  are given in Fig. 6. Fig. 6(a) shows the  $\chi_{\text{SG}}$  data for different system sizes, and the corresponding intersection temperatures data are displayed in Fig. 6(b). The value of the exponent  $\lambda$  for this case is 0.387. The linear fit over the  $T^*(N, 2N)$  data obtained from intersections of  $\chi_{\text{SG}}$ , considering the 6 pairs of largest system sizes, gives  $T_c = 0.5247 \pm 0.0010$  (see Table I).

As for the alternate protocol where we fix the temperature and vary the field, the finite size scaling plots are given in Fig. 7(a). The temperature is fixed at  $T = 0.357 (= 0.680 T_c)$ . A plot of  $h^*(N, 2N)$  versus  $1/N^\lambda$  is in Fig. 7(b), using the same value of  $\lambda = 0.387$ . Omitting the smallest system size, we did a linear fitting over the  $h^*(N, 2N)$  data obtained from  $\chi_{\text{SG}}$  intersections, which gives  $h_{\text{AT}}(T = 0.357) = 0.1150 \pm 0.0030$  (see Table II).

### D. $\sigma = 0.650$

For  $\sigma = 0.650$   $d_{\text{eff}} \approx 6.667$ . Our results for  $h_r = 0$  are given in Fig. 8. The  $\chi_{\text{SG}}$  data for different system sizes are shown in Fig. 8(a). We find the intersection temperatures  $T^*(N, 2N)$  and fit this data with Eq. (18) to find the transition temperature. The exponent  $\lambda \equiv 5/3 - 2\sigma$  is known to equal 0.367 in this case [24, 25]. The result is displayed in Fig. 8(b), where the  $T^*(N, 2N)$  data obtained from intersections of  $\chi_{\text{SG}}$  are fitted against  $N^{-\lambda}$  with a straight line for the largest 7 pairs of system sizes to give  $T_c = 0.5143 \pm 0.0005$  (see Table I).

We have also studied  $\chi_{\text{SG}}$  at fixed temperature  $T = 0.350 (= 0.681 T_c)$ , but varying  $h_r$  and the finite size scaling plots for these are given in Fig. 11(a). A plot of  $h^*(N, 2N)$  versus  $1/N^\lambda$  is in Fig. 9(b), using the same value of  $\lambda = 0.367$ . Omitting the smallest system size, the linear fit from  $\chi_{\text{SG}}$  intersections give  $h_{\text{AT}}(T = 0.350) = 0.1033 \pm 0.0027$  (see Table II).

### E. $\sigma = 0.655$

For  $\sigma = 0.655$   $d_{\text{eff}} \approx 6.452$ . Our results for  $h_r = 0$  are given in Fig. 10. The  $\chi_{\text{SG}}/N^{1/3}$  data are plotted as a function of temperature  $T$  in Fig. 10(a) for different system sizes. We find the temperature  $T^*(N, 2N)$  at which the curves corresponding to the system sizes  $N$  and  $2N$  intersect. We then fit this data with Eq. (18) to find the transition temperature. The exponent  $\lambda \equiv 5/3 - 2\sigma$  is known to equal 0.357 in this case [24, 25]. The result is displayed in Fig. 10(b), where the  $T^*(N, 2N)$  data obtained from intersections of  $\chi_{\text{SG}}$  are fitted against  $N^{-\lambda}$  with a straight line for the largest 3 pairs of system sizes to give  $T_c = 0.5122 \pm 0.0018$  (see Table I).

We have also studied  $\chi_{\text{SG}}$  at fixed  $T = 0.344 (= 0.672 T_c)$ , but varying  $h_r$  and the finite size scaling plots

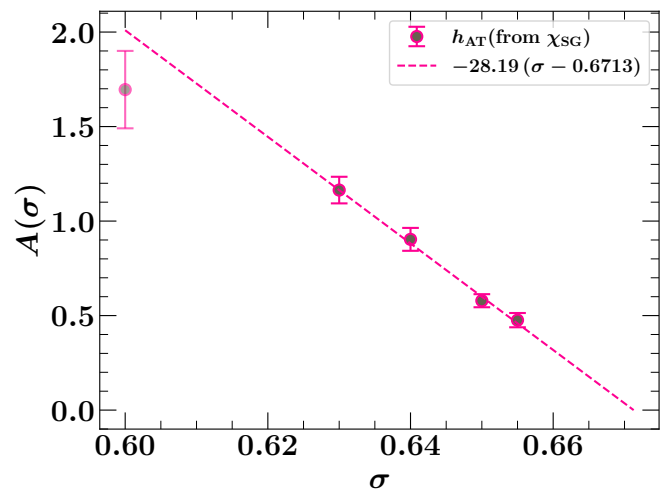


FIG. 12. Plot of  $A(\sigma)$  versus  $\sigma$ . The quantity  $A(\sigma)$  is computed using Eq. (1) with the exponent  $\zeta$  given by Eq. (19) in the mean-field regime. In our simulations we fixed the temperature  $T \approx 0.67 T_c$  and determined the value of the transition field  $h_{\text{AT}}$  from the  $\chi_{\text{SG}}$  data set, (for example see Fig. 5). The  $A(\sigma)$  data (excluding  $\sigma = 0.600$ ) are fitted with a straight line ( $\chi^2/N_{\text{dof}} = 0.351$ ). The line intersects the  $\sigma$ -axis at  $\sigma = 0.671 \pm 0.135$ . In making these linear fits the data point at  $\sigma = 0.600$  has been ignored (hence blurred), as it will lie outside the linear region which only applies for  $\sigma$  values close to  $2/3$ . The error bars are the statistical error bars, but finite size effects produce an unknown systematic error in all the data points.

for these are given in Fig. 11(a). A plot of  $h^*(N, 2N)$  versus  $1/N^\lambda$  is in Fig. 11(b), using the same value of  $\lambda = 0.357$ . Omitting the smallest system size, we did a linear fitting over the  $h^*(N, 2N)$  data obtained from  $\chi_{\text{SG}}$  intersections, which gives  $h_{\text{AT}}(T = 0.344) = 0.1023 \pm 0.0029$  (see Table II).

## V. DISAPPEARANCE OF THE AT LINE AS $\sigma \rightarrow 2/3$

In this section we present our analysis of  $A(\sigma)$  for different values of  $\sigma < 2/3$ , and with the help of this data, we show that the AT line approaches the horizontal axis as we go below six dimensions, or equivalently for  $\sigma > 2/3$ . As shown in Table II, for each  $\sigma$ , we get two estimates of the value of AT transition field  $h_{\text{AT}}$  for a fixed temperature  $T$ ; one from  $\chi_{\text{SG}}$  and one from  $\xi_{\text{SG}}$ . From it, one can extract (using Eq. (1))  $A(\sigma)$  at the values of  $\sigma$  which we have studied. We take the exponent to be:

$$\zeta = \begin{cases} 3, & \sigma < 5/8, \\ \frac{2(1-\sigma)}{2\sigma-1}, & 5/8 < \sigma < 2/3, \end{cases} \quad (19)$$

where we have set  $d = d_{\text{eff}}$  in  $\zeta = d/2 - 1$  for  $\sigma > 5/8$  [6, 7]. We have plotted the results in Fig. 12. Clearly

$A(\sigma)$  is decreasing with increasing  $\sigma$ , and in this linear plot it appears to go to zero when  $\sigma \approx 0.67$ . This is close to the value  $2/3$  which is what would be expected if the AT line disappears in exactly 6 dimensions.

## VI. SUMMARY AND CONCLUSIONS

Due to the challenges associated with performing simulations above six dimensions, we have opted to perform simulations using a one-dimensional proxy model instead. For the one dimensional Heisenberg spin glasses with power-law diluted interactions, we studied five values of  $\sigma < 2/3$ : 0.600, 0.630, 0.640, 0.650, and 0.655.

To find the values of the zero-field spin glass transition temperature  $T_c$ , we performed simulations by varying the temperature  $T$  in the absence of the magnetic field. We then fixed the temperature to  $T \approx 0.67 T_c$  and generated data by varying the magnetic field for different values of  $\sigma$ . The largest system sizes studied are  $N = 32768$  for  $\sigma = 0.600$  and  $0.630$ ,  $N = 16384$  for  $\sigma = 0.640$  and  $0.650$ , and  $N = 65536$  for  $\sigma = 0.655$ . Using the standard finite size scaling analysis we found the values of the AT transition field  $h_{AT}$ , which gave us the values of  $A(\sigma)$ . When  $A(\sigma)$  is studied as a function of  $\sigma$ , we find that it is becoming zero for  $\sigma$  close to  $2/3$ . This is equivalent to saying that  $A(d)$  is vanishing as we approach  $d = 6$  from above six dimensions. The numerical studies reported in this paper imply therefore that the AT line is approaching the temperature axis as  $d \rightarrow 6$ , and hence that there will not be an AT transition below six dimensions.

Numerical studies like this can only provide evidence for what the truth might be: they do not as yet prove it beyond reasonable doubt. The controversy will probably only be ended by a rigorous determination of the lower critical dimension of the AT transition.

## ACKNOWLEDGMENTS

We are grateful to the High Performance Computing (HPC) facility at IISER Bhopal, where large-scale calculations in this project were run. B.V is grateful to the Council of Scientific and Industrial Research (CSIR), India, for his PhD fellowship. A.S acknowledges financial support from SERB via the grant (File Number: CRG/2019/003447), and from DST via the DST-INSPIRE Faculty Award [DST/INSPIRE/04/2014/002461].

### Appendix A: The simulation method

We now describe the technical details of our simulation process. The simulations begin with a random initial configuration, which evolves according to the method outlined in this section. To achieve rapid equilibration, we

use three types of sweeps: overrelaxation (or microcanonical), heatbath, and parallel tempering. In overrelaxation and heatbath sweeps, we flip one spin at a time (single-spin-flip dynamics). To implement parallel tempering, we simulate  $N_T$  copies of the system simultaneously at  $N_T$  different temperatures, ranging from  $T_{\min} \equiv T_1$  to  $T_{\max} \equiv T_{N_T}$ . To facilitate the computation of the observables discussed here, we simulate 4 sets of  $N_T$  copies (2 for  $h_r = 0$ ), labeled (1), (2), (3), and (4). Overrelaxation, heatbath, and parallel tempering sweeps are performed on all copies, with careful tracking of their labels. Every 10 overrelaxation sweeps are followed by 1 heatbath and 1 parallel tempering sweep, as overrelaxation sweeps are computationally cheaper and expedite equilibration. The simulation parameters are listed in Tables BI and BII.

Once equilibrium is reached, we perform an equal number of sweeps in the measurement phase, making  $N_{\text{sweep}}$  the total number of sweeps for the entire simulation, including both equilibration and measurement phases. The last column in the Tables BI and BII indicates the computer time needed to generate the data for each parameter set. The computation time mentioned here indicates the total duration needed to generate all the data using only a single core at a time (with an average clock speed of 2.6 GHz). During the measurement phase, we take one measurement for every 4 sweeps. The following sections provide detailed information on our Monte Carlo simulation procedures.

#### 1. Overrelaxation sweep

We sweep sequentially through all the lattice sites and compute the local field

$$\mathbf{H}_i = \sum_j J_{ij} \mathbf{S}_j + \mathbf{h}_i \quad (\text{A1})$$

at each lattice site. The new spin direction  $\mathbf{S}'_i$  at the  $i^{\text{th}}$  lattice site is taken to be the mirror image of the vector  $\mathbf{S}_i$  about  $\mathbf{H}_i$ , i.e.,

$$\mathbf{S}'_i = -\mathbf{S}_i + 2 \frac{\mathbf{S}_i \cdot \mathbf{H}_i}{H_i^2} \mathbf{H}_i, \quad (\text{A2})$$

where  $H_i = |\mathbf{H}_i|$ . Since  $\mathbf{S}'_i \cdot \mathbf{H}_i = \mathbf{S}_i \cdot \mathbf{H}_i$ , the energy of the system does not change due to these sweeps. Hence these sweeps are also called microcanonical sweeps. These sweeps help us in sampling out the microstates with the same energy. The process of equilibration speeds up when we include overrelaxation sweeps along with the other sweeps [33, 34].

#### 2. Heatbath sweep

The microcanonical sweep samples out microstates from the state-space with same energy. But, to equilibrate the system, we have to sample out the states  $\{\mathbf{S}_i\}$

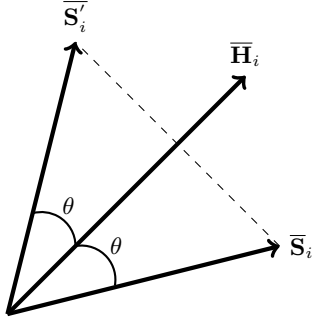


FIG. A1. The vector  $\mathbf{H}_i$  is the local-field at the site  $i$  which is the effective field felt by the spin  $\mathbf{S}_i$  due to its interaction with all other spins. The vector  $\mathbf{S}'_i$  is the reflection of  $\mathbf{S}_i$  about  $\mathbf{H}_i$  determined by Eq. (A2)

with different energies according to the correct Boltzmann weight  $\exp(-\beta\mathcal{H}(\{\mathbf{S}_i\}))/Z$ , where  $\beta = 1/T$  is the inverse temperature and  $Z$  is the partition function. Therefore, we perform a heatbath sweep for every 10 microcanonical sweeps [33, 34]. Similar to the microcanonical case, we sweep sequentially through the lattice and compute the local field vector  $\mathbf{H}_i$  given by Eq. (A1). We can define a coordinate system with  $\mathbf{H}_i$  as polar axis,  $\theta$  as polar angle, and  $\phi$  as azimuthal angle, such that  $\phi = 0$  for the old spin vector  $\mathbf{S}_i$  (see Fig. A1). The contribution of the  $i^{\text{th}}$  spin to the total energy of the system is given by  $E_i = -\mathbf{H}_i \cdot \mathbf{S}_i = -H_i S_i \cos \theta$  (since we are considering spins of unit length  $S_i = |\mathbf{S}_i| = 1$ ). For the new spin direction  $\mathbf{S}'_i(\theta, \phi)$ , since the energy does not depend on  $\phi$ , we pick it uniformly from the interval  $(0, 2\pi)$ , and sample out  $\theta$  from the probability distribution

$$f_X(x = \cos \theta) = \frac{e^{-\beta E_i}}{Z} = \frac{\beta H_i S_i}{2 \sinh \beta H_i S_i} e^{\beta H_i S_i x}. \quad (\text{A3})$$

The simplest way to do this is to equate the cumulative distributive function (CDF) of  $x = \cos \theta$ ,  $F_X(x)$ , to that of a uniform distribution:

$$F_X(x) = \int_{-1}^x f_X(x') dx' = \Pi(r_2) = \int_0^{r_2} dr = r_2, \quad (\text{A4})$$

where  $r_2$  is a random variable sampled from a uniform distribution in the interval  $(0, 1)$ . Upon simplifying Eq. (A4), we get

$$x = \cos \theta = \frac{1}{\beta H_i S_i} \ln [1 + r_2 (e^{2\beta H_i S_i} - 1)] - 1. \quad (\text{A5})$$

To find the components of the spin vector  $\mathbf{S}'_i$  in the original Cartesian coordinates, we perform a rotation about Y-axis by  $\theta_H$  in the anti-clockwise direction, and then about Z-axis by  $\phi_H$  in the clockwise direction, where  $\theta_H$  and  $\phi_H$  are the polar and azimuthal angles of  $\mathbf{H}_i$  relative

to the Cartesian reference frame, i.e.,

$$\begin{pmatrix} S'_x \\ S'_y \\ S'_z \end{pmatrix} = R_Z(-\phi_H) R_Y(\theta_H) \begin{pmatrix} \sin \theta \cos \phi \\ \sin \theta \sin \phi \\ \cos \theta \end{pmatrix}, \quad (\text{A6})$$

where

$$R_Y(\theta_H) = \begin{pmatrix} \cos \theta_H & 0 & \sin \theta_H \\ 0 & 1 & 0 \\ -\sin \theta_H & 0 & \cos \theta_H \end{pmatrix}, \quad (\text{A7})$$

$$R_Z(-\phi_H) = \begin{pmatrix} \cos \phi_H & -\sin \phi_H & 0 \\ \sin \phi_H & \cos \phi_H & 0 \\ 0 & 0 & 1 \end{pmatrix}. \quad (\text{A8})$$

The acceptance probability for both heatbath sweeps and microcanonical sweeps is unity, ensuring that no moves are wasted.

### 3. Parallel tempering sweep

Spin glasses exhibit a complex free energy landscape, causing them to become trapped in metastable valleys at low temperatures, making true equilibration very time-consuming. At higher temperatures, thermal fluctuations allow the system to escape these valleys easily, resulting in quicker equilibration. To achieve equilibrium with the fewest moves, we perform one parallel tempering sweep for every 10 overrelaxation sweeps [33, 35]. To benefit from the parallel tempering algorithm [36, 37], we simultaneously simulate  $N_T$  copies of the system at  $N_T$  different temperatures  $T_1 < T_2 < T_3 < \dots < T_{N_T}$ . The minimum temperature  $T_1$  is the low temperature of interest for studying system behavior, while the maximum temperature  $T_{N_T}$  is sufficiently high for rapid equilibration. Overrelaxation and heatbath sweeps are performed separately on each of the  $N_T$  copies of the system. In the parallel tempering sweep, we compare the energies of two spin configurations at adjacent temperatures,  $T_i$  and  $T_{i+1}$ , starting from the smallest temperature  $T_1$ . We swap these two spin configurations such that the detailed balance condition is satisfied. The Metropolis probability for such a swap is

$$P(T \text{ swap}) = \min\{1, \exp(\Delta\beta\Delta E)\} \quad (\text{A9})$$

$$= \begin{cases} \exp(\Delta\beta\Delta E), & (\text{if } \Delta\beta\Delta E < 0), \\ 1, & (\text{otherwise}), \end{cases} \quad (\text{A10})$$

where  $\Delta\beta = 1/T_i - 1/T_{i+1}$  and  $\Delta E = E_i(T_i) - E_{i+1}(T_{i+1})$ . In this way, a given set of spins performs a random walk in temperature space.

### 4. Checks for equilibration

In order to check whether the system has reached equilibrium, we have used a convenient test [38] which is pos-

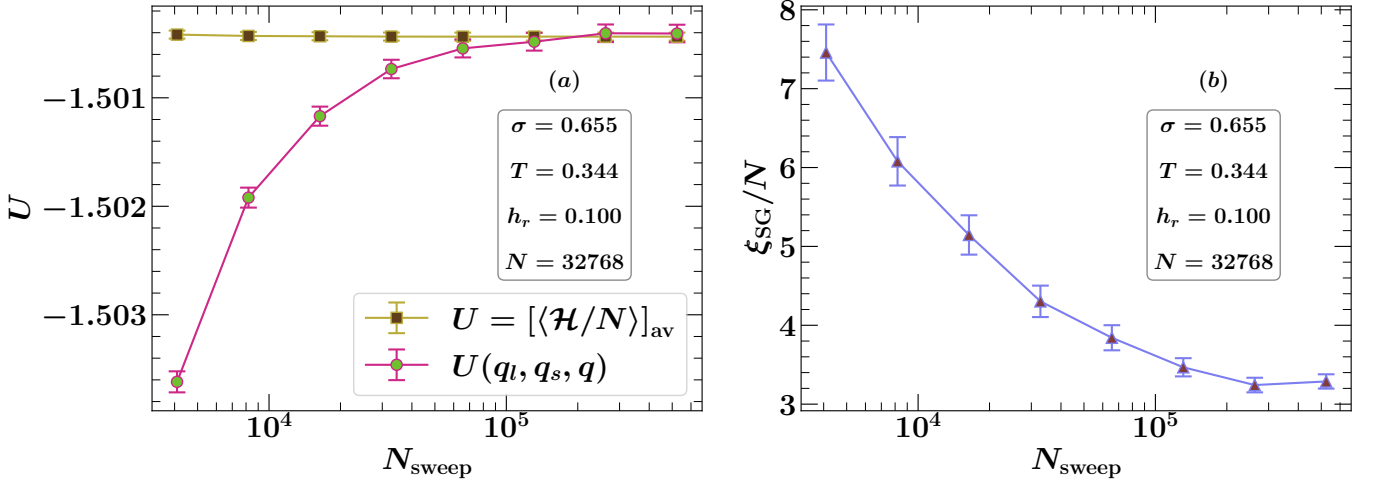


FIG. A2. The plot illustrates the test for equilibration. In (a), the energy ( $U$ ) is plotted as a function of Monte Carlo sweeps. The brown curve, labeled  $U = [\langle \mathcal{H}/N \rangle]_{\text{av}}$ , is derived from Eq. (A12), while the pink curve represents  $U(q_l, q_s, q)$  calculated from the right-hand side of Eq. (A11). As evident from the plot, both quantities converge to the same value after  $10^5$  sweeps. Once this common point is reached, the curves flatten and remain constant over time, indicating that the system has achieved thermal equilibrium. To reinforce our test, we also analyzed  $\xi_{\text{SG}}/N$  as a function of  $N_{\text{sweep}}$ , shown in (b). This figure demonstrates that the  $\xi_{\text{SG}}$  data becomes constant at the  $N_{\text{sweep}}$  value where the curves in (a) converge. The data presented here are for a specific set of parameters. We repeated this test for all parameter sets listed in Tables BI and BII, and proceeded with measurements only after confirming the system had properly equilibrated.

sible because of the Gaussian nature of the interactions and the onsite external magnetic field. The relation

$$U = \frac{zJ^2}{2T} (q_l - q_s) + \frac{h_r^2}{T} (q - |\mathbf{S}|^2), \quad (\text{A11})$$

is valid in equilibrium. Here

$$U = \frac{1}{N} [\langle \mathcal{H} \rangle]_{\text{av}} = -\frac{1}{N} \left[ \sum_{\langle i,j \rangle} \epsilon_{ij} J_{ij} \langle \mathbf{S}_i \cdot \mathbf{S}_j \rangle + \sum_{i,\mu} h_i^\mu \langle S_i^\mu \rangle \right]_{\text{av}} \quad (\text{A12})$$

is the average energy per spin,  $q = \frac{1}{N} \sum_i [\langle \mathbf{S}_i \cdot \mathbf{S}_i \rangle]_{\text{av}}$  is the Edwards-Anderson order parameter,  $q_l = \frac{1}{N_b} \sum_{\langle i,j \rangle} [\epsilon_{ij} \langle \mathbf{S}_i \cdot \mathbf{S}_j \rangle^2]_{\text{av}}$  is the “link overlap”, and  $q_s = \frac{1}{N_b} \sum_{\langle i,j \rangle} [\epsilon_{ij} \langle (\mathbf{S}_i \cdot \mathbf{S}_j)^2 \rangle]_{\text{av}}$  is the “spin overlap”, where

$N_b = Nz/2$ , and  $\epsilon_{ij} = 1$  if the  $i^{\text{th}}$  and  $j^{\text{th}}$  spins are interacting and is zero otherwise. As the system reaches equilibrium, the two sides of Eq. (A11) approach their common equilibrium value from opposite directions.

In simulations, we assess both sides of Eq.(A11) for various numbers of Monte Carlo sweeps (MCSs), which increase exponentially, with each value being double the previous one. Averaging is done over the last half of the sweeps. Starting with a random spin configuration, the LHS of Eq.(A11) is initially small, and the RHS is very large. As the system nears equilibrium, these values converge from opposite directions, as illustrated in Fig. A2(a). We declare the system to have reached equilibrium when the averaged quantities consistently satisfy Eq. (A11) within error bars for at least the last two points. Once equilibrium is achieved, we perform an equal number of sweeps in the measurement phase, where we evaluate various quantities to study potential phase transitions in the system. To further strengthen our equilibration check, we analysed  $\xi_{\text{SG}}$  as a function of the Monte Carlo sweeps. Our data in Fig. A2(b) show that the  $\xi_{\text{SG}}$  curve flattens off for the same number of sweeps where the two sides of Eq. (A11) start to agree.

### Appendix B: Parameters of the simulations

TABLE BI. Parameters of the simulations.  $N_{\text{samp}}$  is the number of disorder samples,  $N_{\text{sweep}}$  is the number of over-relaxation Monte Carlo sweeps for a single disorder sample. The system is equilibrated over the first half of the sweeps, and measurements are done over the last half of the sweeps with a measurement performed every four over-relaxation sweeps.  $T_{\text{min}}$  and  $T_{\text{max}}$  are the lowest and highest temperatures simulated, and  $N_T$  is the number of temperatures used for parallel tempering.  $t_{\text{tot}}$  is the total CPU time consumed in hours to generate data for a particular system size.

$\sigma$	$h_r$	$N$	$N_{\text{samp}}$	$N_{\text{sweep}}$	$T_{\text{min}}$	$T_{\text{max}}$	$N_T$	$t_{\text{tot}}$ (hrs)
0.6	0	128	12000	256	0.2	0.7	40	1.2
0.6	0	256	12000	512	0.2	0.7	40	4.89
0.6	0	512	12000	1024	0.2	0.7	40	21.57
0.6	0	1024	12000	2048	0.2	0.7	40	48.58
0.6	0	2048	9600	4096	0.2	0.7	40	235.21
0.6	0	4096	7200	8192	0.3	0.7	40	1109.96
0.6	0	8192	3120	16384	0.3	0.7	50	2611.03
0.6	0	16384	1200	32768	0.35	0.7	55	6453.1
0.6	0	32768	408	65536	0.35	0.7	60	7663.65
0.63	0	128	8000	512	0.2	0.7	40	1.24
0.63	0	256	8000	1024	0.2	0.7	40	5.81
0.63	0	512	8000	2048	0.2	0.7	40	29.16
0.63	0	1024	8000	8192	0.2	0.7	40	191.87
0.63	0	2048	8000	8192	0.3	0.7	40	460.11
0.63	0	4096	4560	16384	0.32	0.68	40	1156.2
0.63	0	8192	3193	32768	0.36	0.66	42	6183.85
0.63	0	16384	2432	32768	0.38	0.66	44	9954.44
0.64	0	128	24000	512	0.2	0.7	40	3.14
0.64	0	256	24000	1024	0.2	0.7	40	17.33
0.64	0	512	22400	2048	0.2	0.7	40	70.61
0.64	0	1024	11200	8192	0.2	0.7	40	305.41
0.64	0	2048	16000	8192	0.3	0.7	40	815.66
0.64	0	4096	12000	16384	0.32	0.68	40	3751.7
0.64	0	8192	3360	32768	0.36	0.66	42	6323.48
0.64	0	16384	2240	32768	0.38	0.66	44	9724.53
0.65	0	128	9600	512	0.3	0.7	40	1.96
0.65	0	256	9600	1024	0.3	0.7	40	7.83
0.65	0	512	9600	2048	0.3	0.7	40	32.98
0.65	0	1024	33600	4096	0.3	0.7	44	457.63
0.65	0	2048	33600	8192	0.3	0.7	40	2212.92
0.65	0	4096	19200	16384	0.32	0.68	40	6242.19
0.65	0	8192	15054	16384	0.36	0.66	42	14652.7
0.65	0	16384	10526	32768	0.38	0.66	44	42378.9
0.655	0	128	24000	512	0.2	0.7	40	3.05
0.655	0	256	24000	1024	0.2	0.7	40	14.69
0.655	0	512	16000	2048	0.2	0.7	40	43.48
0.655	0	1024	21920	4096	0.3	0.7	40	291.4
0.655	0	2048	20400	8192	0.3	0.7	40	1143.21
0.655	0	4096	18252	16384	0.32	0.68	40	6818.29
0.655	0	8192	12260	16384	0.36	0.66	42	11835.9
0.655	0	16384	5278	32768	0.38	0.66	44	22993.1
0.655	0	32768	3646	32768	0.38	0.66	44	29010.7

TABLE BII. Parameters of the simulations done at fixed temperature  $T$  and varying field  $h_r$ .  $N(h_r)$  is the number of values of field taken in the range  $h_r(\text{min,max})$ . The equilibration times are different for different values of the field  $h_r$ , which lie in the range  $N_{\text{sweep}}(\text{min,max})$ . The number of disorder samples for different fields lie in the range  $N_{\text{samp}}(\text{min,max})$ .  $t_{\text{tot}}$  is the total CPU time consumed in hours to generate data for a particular system size.

$\sigma$	$T$	$N$	$h_r(\text{min,max})$	$N(h_r)$	$N_{\text{sweep}}(\text{min,max})$	$N_{\text{samp}}(\text{min,max})$	$t_{\text{tot}}(\text{hrs})$
0.6	0.38	128	(0.0100, 9.0000)	27	(1024, 1024)	(5000, 20000)	2.55
0.6	0.38	256	(0.0100, 9.0000)	27	(2048, 2048)	(5000, 30000)	18.5
0.6	0.38	512	(0.0100, 9.0000)	27	(2048, 2048)	(5000, 30000)	40.78
0.6	0.38	1024	(0.0100, 9.0000)	30	(4096, 4096)	(4000, 30000)	181.68
0.6	0.38	2048	(0.0100, 9.0000)	31	(4096, 8192)	(2500, 40000)	3506.91
0.6	0.38	4096	(0.0100, 9.0000)	31	(8192, 32768)	(4000, 75200)	9948.45
0.6	0.38	8192	(0.0100, 9.0000)	27	(16384, 262144)	(1200, 37050)	88881.3
0.6	0.38	16384	(0.0100, 9.0000)	29	(32768, 524288)	(240, 12749)	151254
0.6	0.38	32768	(0.1000, 0.1400)	3	(131072, 1048576)	(3813, 7596)	155371
0.63	0.364	128	(0.0100, 9.0000)	28	(512, 512)	(4000, 16000)	2.07
0.63	0.364	256	(0.0100, 9.0000)	33	(1024, 1024)	(4000, 32000)	16.06
0.63	0.364	512	(0.0100, 9.0000)	34	(2048, 2048)	(4000, 32000)	52.31
0.63	0.364	1024	(0.0100, 9.0000)	33	(4096, 4096)	(5000, 32000)	200.35
0.63	0.364	2048	(0.0100, 9.0000)	33	(4096, 8192)	(4000, 36000)	967.71
0.63	0.364	4096	(0.0100, 9.0000)	32	(8192, 32768)	(4000, 37440)	7357.41
0.63	0.364	8192	(0.0100, 9.0000)	33	(16384, 131072)	(643, 34251)	56078.5
0.63	0.364	16384	(0.0100, 9.0000)	30	(32768, 524288)	(640, 18941)	94942.1
0.63	0.364	32768	(0.0900, 0.1200)	4	(262144, 524288)	(4892, 14287)	159218
0.64	0.357	128	(0.0100, 9.0000)	27	(1024, 1024)	(5000, 40000)	4.56
0.64	0.357	256	(0.0100, 9.0000)	27	(2048, 2048)	(2000, 40000)	19.01
0.64	0.357	512	(0.0400, 9.0000)	25	(2048, 2048)	(2000, 50000)	48.42
0.64	0.357	1024	(0.0100, 9.0000)	28	(4096, 4096)	(2000, 40000)	190.31
0.64	0.357	2048	(0.0100, 9.0000)	28	(4096, 8192)	(1000, 40000)	791.55
0.64	0.357	4096	(0.0400, 9.0000)	25	(8192, 16384)	(1000, 36000)	4250.85
0.64	0.357	8192	(0.0100, 9.0000)	28	(16384, 131072)	(1600, 37120)	23608.4
0.64	0.357	16384	(0.0100, 9.0000)	28	(32768, 262144)	(320, 12800)	58060.3
0.65	0.35	128	(0.0100, 9.0000)	29	(1024, 1024)	(4000, 12000)	10.12
0.65	0.35	256	(0.0100, 9.0000)	29	(2048, 2048)	(4000, 12000)	14.64
0.65	0.35	512	(0.0100, 9.0000)	29	(4096, 4096)	(4000, 12000)	58.13
0.65	0.35	1024	(0.0100, 0.3000)	14	(8192, 8192)	(4000, 10000)	139.38
0.65	0.35	2048	(0.0100, 0.3000)	14	(16384, 16384)	(4800, 24000)	800.5
0.65	0.35	4096	(0.0100, 9.0000)	29	(32768, 32768)	(1200, 24000)	4786.42
0.65	0.35	8192	(0.0100, 0.3000)	14	(65536, 131072)	(800, 21551)	27908.2
0.65	0.35	16384	(0.0100, 0.3000)	14	(262144, 262144)	(551, 11602)	74407.7
0.655	0.344	128	(0.0100, 9.0000)	27	(1024, 1024)	(4000, 44000)	6.03
0.655	0.344	256	(0.0100, 9.0000)	29	(2048, 2048)	(4000, 44000)	30.18
0.655	0.344	512	(0.0100, 9.0000)	29	(4096, 4096)	(2000, 60000)	80.09
0.655	0.344	1024	(0.0100, 9.0000)	30	(8192, 8192)	(2000, 48000)	265.81
0.655	0.344	2048	(0.0100, 9.0000)	30	(16384, 16384)	(1000, 41600)	1838.4
0.655	0.344	4096	(0.0100, 9.0000)	29	(16384, 32768)	(960, 36960)	7440.49
0.655	0.344	8192	(0.0100, 9.0000)	32	(16384, 65536)	(480, 42800)	42173.3
0.655	0.344	16384	(0.0100, 9.0000)	32	(32768, 262144)	(576, 20479)	191977
0.655	0.344	32768	(0.0100, 9.0000)	29	(65536, 524288)	(256, 14707)	272176
0.655	0.344	65536	(0.0100, 0.2000)	8	(524288, 1048576)	(192, 3845)	245877

### Appendix C: $\xi_{\text{SG}}$ data

We believe that the results for  $h_{\text{AT}}$  derived from  $\xi_{\text{SG}}$  data are badly affected by finite size effects and are thus less reliable than the values obtained from  $\chi_{\text{SG}}$ , possibly for the reasons given at the end of Sec. III. That is why these analyses have been relegated to this Appendix.

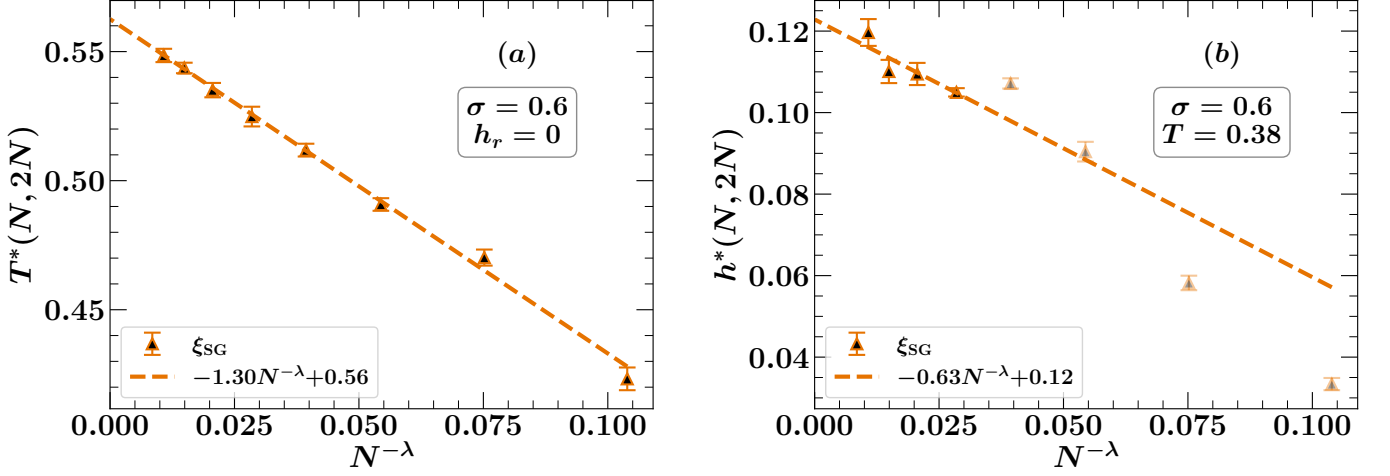


FIG. C1. Plots showing (a)  $T^*(N, 2N)$  and (b)  $h^*(N, 2N)$  data obtained from  $\xi_{\text{SG}}$  as a function of  $N^{-\lambda}$  for  $\sigma = 0.600$ . The value of  $\lambda = 0.467$  used here is the same as the value used for the corresponding  $\chi_{\text{SG}}$  data in Figs. 2(b) and 3(b). Both the data sets are fitted with a straight line and the resulting values are  $T_c = 0.5626 \pm 0.0017$  from (a) and  $h_{\text{AT}}(T = 0.380) = 0.1229 \pm 0.0038$  from (b). The blurred points in (b) are excluded from the linear fitting.

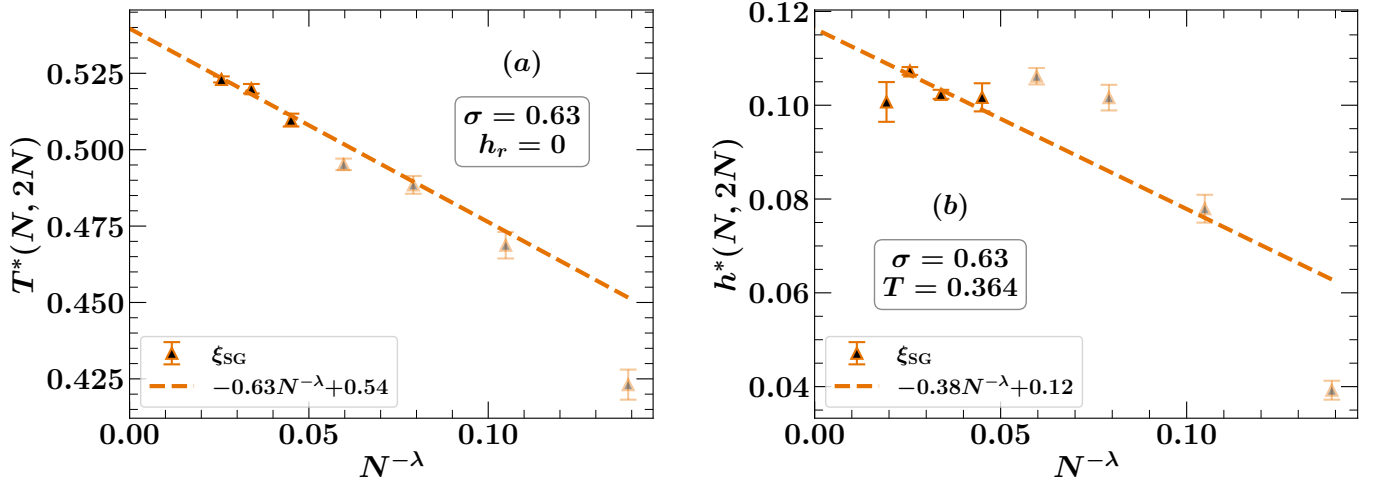


FIG. C2. Plots showing (a)  $T^*(N, 2N)$  and (b)  $h^*(N, 2N)$  data obtained from  $\xi_{\text{SG}}$  as a function of  $N^{-\lambda}$  for  $\sigma = 0.630$ . The value of  $\lambda = 0.407$  used here is the same as the value used for the corresponding  $\chi_{\text{SG}}$  data in Figs. 4(b) and 5(b). Both the data sets are fitted with a straight line and the resulting values are  $T_c = 0.5396 \pm 0.0035$  from (a) and  $h_{\text{AT}}(T = 0.364) = 0.1164 \pm 0.0035$  from (b). The blurred points in (a) and (b) are excluded from the linear fitting.



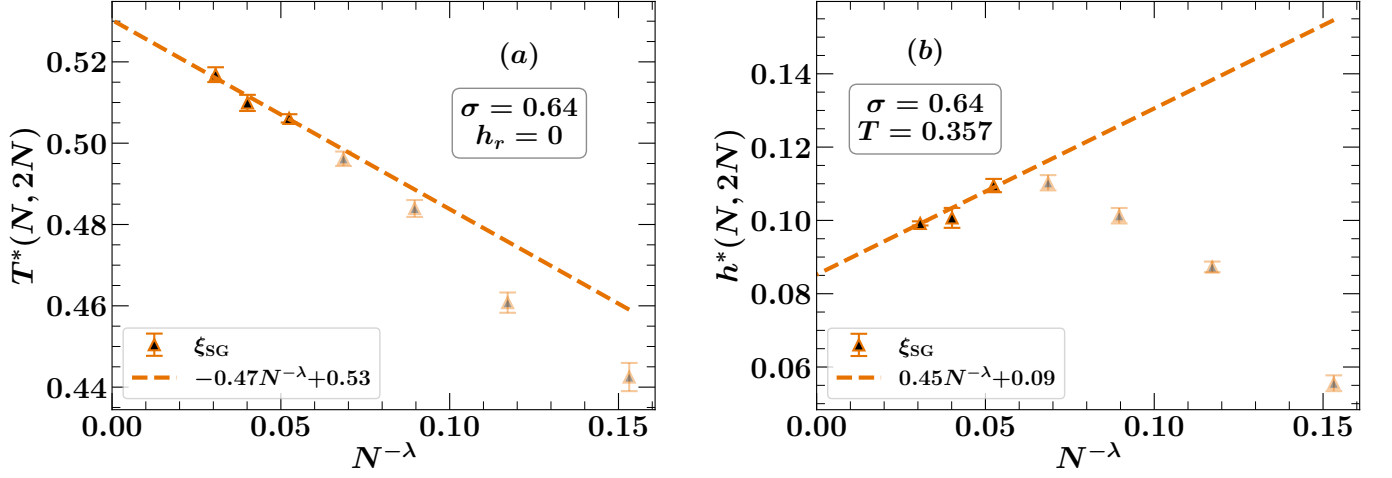


FIG. C3. Plots showing (a)  $T^*(N, 2N)$  and (b)  $h^*(N, 2N)$  data obtained from  $\xi_{SG}$  as a function of  $N^{-\lambda}$  for  $\sigma = 0.640$ . The value of  $\lambda = 0.387$  used here is the same as the value used for the corresponding  $\chi_{SG}$  data in Figs. 6(b) and 7(b). Both the data sets are fitted with a straight line and the resulting values are  $T_c = 0.5303 \pm 0.0043$  from (a) and  $h_{AT}(T = 0.357) = 0.0852 \pm 0.0028$  from (b). The blurred points in (a) and (b) are excluded from the linear fitting.

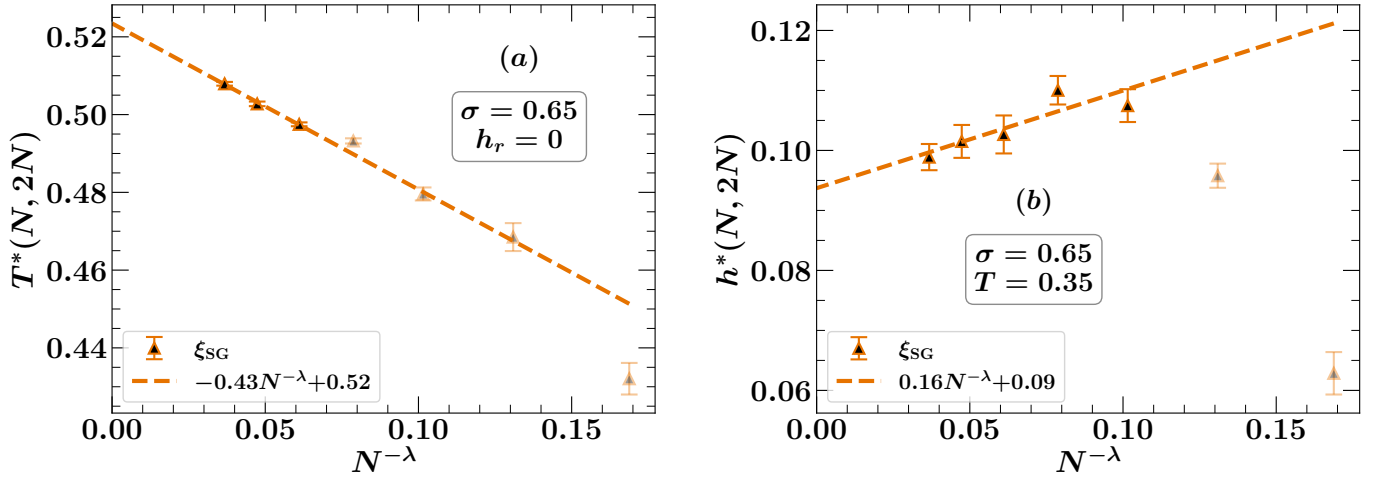


FIG. C4. Plots showing (a)  $T^*(N, 2N)$  and (b)  $h^*(N, 2N)$  data obtained from  $\xi_{SG}$  as a function of  $N^{-\lambda}$  for  $\sigma = 0.650$ . The value of  $\lambda = 0.367$  used here is the same as the value used for the corresponding  $\chi_{SG}$  data in Figs. 8(b) and 9(b). Both the data sets are fitted with a straight line and the resulting values are  $T_c = 0.5235 \pm 0.0014$  from (a) and  $h_{AT}(T = 0.350) = 0.0937 \pm 0.0033$  from (b). The blurred points in (a) and (b) are excluded from the linear fitting.

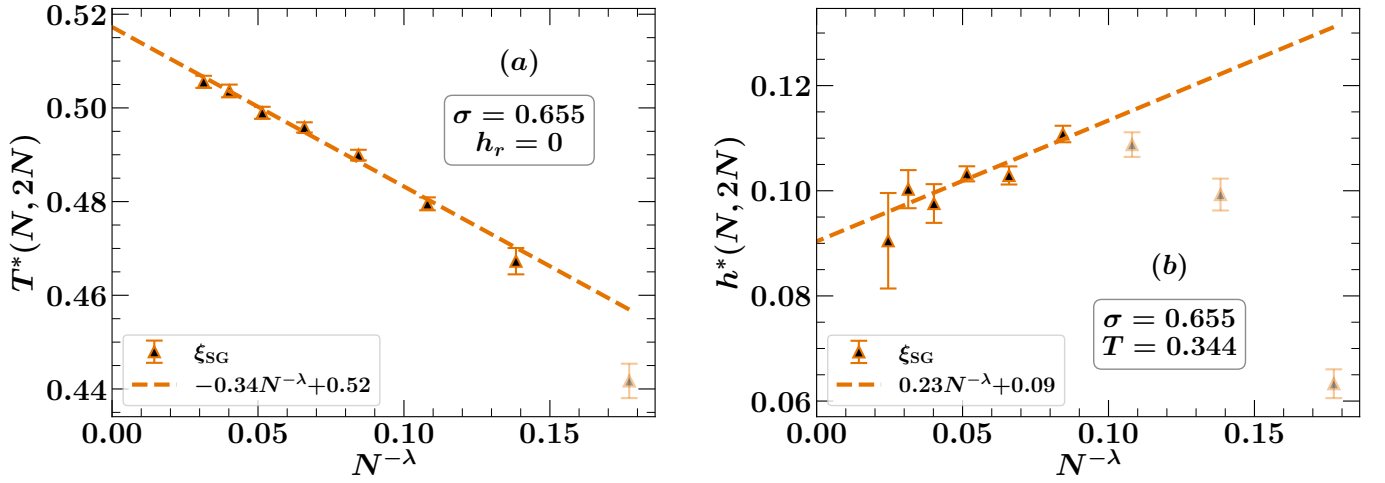


FIG. C5. Plots showing (a)  $T^*(N, 2N)$  and (b)  $h^*(N, 2N)$  data obtained from  $\xi_{SG}$  as a function of  $N^{-\lambda}$  for  $\sigma = 0.655$ . The value of  $\lambda = 0.357$  used here is the same as the value used for the corresponding  $\chi_{SG}$  data in Figs. 10(b) and 11(b). Both the data sets are fitted with a straight line and the resulting values are  $T_c = 0.5173 \pm 0.0013$  from (a) and  $h_{AT}(T = 0.344) = 0.0904 \pm 0.0033$  from (b). The blurred points in (a) and (b) are excluded from the linear fitting.

- 
- [1] G. Parisi, “Toward a mean field theory for spin glasses,” *Physics Letters A* **73**, 203–205 (1979).
- [2] Marc Mézard, Giorgio Parisi, and Miguel Angel Virasoro, *Spin glass theory and beyond: An Introduction to the Replica Method and Its Applications*, Vol. 9 (World Scientific Publishing Company, 1986).
- [3] A J Bray and S A Roberts, “Renormalisation-group approach to the spin glass transition in finite magnetic fields,” *Journal of Physics C: Solid State Physics* **13**, 5405 (1980).
- [4] J R L de Almeida and D J Thouless, “Stability of the Sherrington-Kirkpatrick solution of a spin glass model,” *Journal of Physics A: Mathematical and General* **11**, 983–990 (1978).
- [5] David Sherrington and Scott Kirkpatrick, “Solvable Model of a Spin-Glass,” *Phys. Rev. Lett.* **35**, 1792–1796 (1975).
- [6] J E Green, M A Moore, and A J Bray, “Upper critical dimension for the de Almeida-Thouless instability in spin glasses,” *Journal of Physics C: Solid State Physics* **16**, L815 (1983).
- [7] Daniel S. Fisher and H. Sompolinsky, “Scaling in Spin-Glasses,” *Phys. Rev. Lett.* **54**, 1063–1066 (1985).
- [8] A. B. Harris, T. C. Lubensky, and Jing-Huei Chen, “Critical Properties of Spin-Glasses,” *Phys. Rev. Lett.* **36**, 415–418 (1976).
- [9] Auditya Sharma and A. P. Young, “de Almeida–Thouless line in vector spin glasses,” *Phys. Rev. E* **81**, 061115 (2010).
- [10] M A Moore and A J Bray, “The nature of the spin-glass phase and finite size effects,” *Journal of Physics C: Solid State Physics* **18**, L699 (1985).
- [11] Joonhyun Yeo and M. A. Moore, “Critical point scaling of Ising spin glasses in a magnetic field,” *Phys. Rev. B* **91**, 104432 (2015).
- [12] T. Aspelmeier, M. A. Moore, and A. P. Young, “Interface Energies in Ising Spin Glasses,” *Phys. Rev. Lett.* **90**, 127202 (2003).
- [13] T. Aspelmeier, Wenlong Wang, M. A. Moore, and Helmut G. Katzgraber, “Interface free-energy exponent in the one-dimensional Ising spin glass with long-range interactions in both the droplet and broken replica symmetry regions,” *Phys. Rev. E* **94**, 022116 (2016).
- [14] A. C. Carter, A. J. Bray, and M. A. Moore, “Aspect-Ratio Scaling and the Stiffness Exponent  $\theta$  for Ising Spin Glasses,” *Phys. Rev. Lett.* **88**, 077201 (2002).
- [15] Alexander K. Hartmann, Alan J. Bray, A. C. Carter, M. A. Moore, and A. P. Young, “Stiffness exponent of two-dimensional Ising spin glasses for nonperiodic boundary conditions using aspect-ratio scaling,” *Phys. Rev. B* **66**, 224401 (2002).
- [16] Wenlong Wang, M. A. Moore, and Helmut G. Katzgraber, “Fractal dimension of interfaces in Edwards-Anderson spin glasses for up to six space dimensions,” *Phys. Rev. E* **97**, 032104 (2018).
- [17] Stefan Boettcher, “Stiffness of the Edwards-Anderson Model in all Dimensions,” *Phys. Rev. Lett.* **95**, 197205 (2005).
- [18] M. A. Moore, “ $1/m$  expansion in spin glasses and the de Almeida-Thouless line,” *Phys. Rev. E* **86**, 031114 (2012).
- [19] J. Mattsson, T. Jonsson, P. Nordblad, H. Aruga Katori, and A. Ito, “No Phase Transition in a Magnetic Field in the Ising Spin Glass  $\text{Fe}_{0.5}\text{Mn}_{0.5}\text{TiO}_3$ ,” *Phys. Rev. Lett.* **74**, 4305–4308 (1995).
- [20] V. S. Zotev, G. G. Kenning, and R. Orbach, “From linear to nonlinear response in spin glasses: Importance of mean-field-theory predictions,” *Phys. Rev. B* **66**, 014412 (2002).
- [21] V. Martin-Mayor, J. J. Ruiz-Lorenzo, B. Seoane, and A. P. Young, “Numerical Simulations and Replica Symmetry Breaking,” (2022), [arXiv:2205.14089](https://arxiv.org/abs/2205.14089) [cond-

- mat.dis-nn].
- [22] M. Aguilar-Janita, V. Martin-Mayor, J. Moreno-Gordo, and J. J. Ruiz-Lorenzo, “Evidence of a second-order phase transition in the six-dimensional Ising spin glass in a field,” *Phys. Rev. E* **109**, 055302 (2024).
- [23] Bharadwaj Vedula, M. A. Moore, and Auditya Sharma, “Study of the de Almeida–Thouless line in the one-dimensional diluted power-law  $XY$  spin glass,” *Phys. Rev. E* **108**, 014116 (2023).
- [24] Auditya Sharma and A. P. Young, “Phase transitions in the one-dimensional long-range diluted Heisenberg spin glass,” *Phys. Rev. B* **83**, 214405 (2011).
- [25] Derek Larson, Helmut G. Katzgraber, M. A. Moore, and A. P. Young, “Numerical studies of a one-dimensional three-spin spin-glass model with long-range interactions,” *Phys. Rev. B* **81**, 064415 (2010).
- [26] Helmut G. Katzgraber and A. P. Young, “Monte Carlo studies of the one-dimensional Ising spin glass with power-law interactions,” *Phys. Rev. B* **67**, 134410 (2003).
- [27] L. Leuzzi, G. Parisi, F. Ricci-Tersenghi, and J. J. Ruiz-Lorenzo, “Dilute One-Dimensional Spin Glasses with Power Law Decaying Interactions,” *Phys. Rev. Lett.* **101**, 107203 (2008).
- [28] L. W. Lee and A. P. Young, “Large-scale Monte Carlo simulations of the isotropic three-dimensional Heisenberg spin glass,” *Phys. Rev. B* **76**, 024405 (2007).
- [29] Derek Larson, Helmut G. Katzgraber, M. A. Moore, and A. P. Young, “Numerical studies of a one-dimensional three-spin spin-glass model with long-range interactions,” *Phys. Rev. B* **81**, 064415 (2010).
- [30] L. Leuzzi, G. Parisi, F. Ricci-Tersenghi, and J. J. Ruiz-Lorenzo, “Ising Spin-Glass Transition in a Magnetic Field Outside the Limit of Validity of Mean-Field Theory,” *Phys. Rev. Lett.* **103**, 267201 (2009).
- [31] Auditya Sharma and A. P. Young, “de Almeida–Thouless line studied using one-dimensional power-law diluted Heisenberg spin glasses,” *Phys. Rev. B* **84**, 014428 (2011).
- [32] T. Aspelmeier, Helmut G. Katzgraber, Derek Larson, M. A. Moore, Matthew Wittmann, and Joonhyun Yeo, “Finite-size critical scaling in Ising spin glasses in the mean-field regime,” *Phys. Rev. E* **93**, 032123 (2016).
- [33] J. H. Pixley and A. P. Young, “Large-scale Monte Carlo simulations of the three-dimensional  $XY$  spin glass,” *Phys. Rev. B* **78**, 014419 (2008).
- [34] J. L. Alonso, A. Tarancón, H. G. Ballesteros, L. A. Fernández, V. Martín-Mayor, and A. Muñoz Sudupe, “Monte Carlo study of  $O(3)$  antiferromagnetic models in three dimensions,” *Phys. Rev. B* **53**, 2537–2545 (1996).
- [35] L. W. Lee and A. P. Young, “Large-scale Monte Carlo simulations of the isotropic three-dimensional Heisenberg spin glass,” *Phys. Rev. B* **76**, 024405 (2007).
- [36] Koji Hukushima and Koji Nemoto, “Exchange monte carlo method and application to spin glass simulations,” *Journal of the Physical Society of Japan* **65**, 1604–1608 (1996).
- [37] J. Machta, “Strengths and weaknesses of parallel tempering,” *Phys. Rev. E* **80**, 056706 (2009).
- [38] Helmut G. Katzgraber, Matteo Palassini, and A. P. Young, “Monte Carlo simulations of spin glasses at low temperatures,” *Phys. Rev. B* **63**, 184422 (2001).